Application of the Pseudo-Global Warming Approach in a Kilometer-Resolution Climate Simulation of the Tropics

Christoph Heim[1], David Leutwyler[2], and Christoph Schär[3]

[1]ETH Zürich
[2]Unknown
[3]ETH Zurich

November 26, 2022

Abstract

Clouds over tropical oceans are an important factor in Earth's response to increased greenhouse gas concentrations, but their representation in climate models is challenging due to the small-scale nature of the involved convective processes. We perform two 4-year-long simulations at kilometer-resolution (3.3 km horizontal grid spacing) with the limited-area model COSMO over the tropical Atlantic on a 9000x7000 km2 domain: A control simulation under current climate conditions driven by the ERA5 reanalysis, and a climate change scenario simulation using the Pseudo-Global Warming (PGW) approach. We compare these results to the changes projected in the CMIP6 scenario ensemble. We find a good representation of the annual cycle of albedo, in particular for trade-wind clouds, even compared to the ERA5 reanalysis. Also, the vertical structure and annual cycle of the marine intertropical convergence zone (ITCZ) is accurately simulated, and the simulation does not suffer from the double ITCZ problem commonly present in global climate models (GCMs). The ITCZ responds to warming through a vertical extension and intensification primarily at high levels, as well as a slight southward extension of the annual mean ITCZ, while the narrowing typically seen in GCMs is not visible.

Application of the Pseudo-Global Warming Approach in a Kilometer-Resolution Climate Simulation of the Tropics

Christoph Heim[1], David Leutwyler[1], Christoph Schär[1]

[1]Institute for Atmospheric and Climate Science, ETH Zurich, Zürich, Switzerland

Key Points:

- We perform a kilometer-resolution climate simulation over the tropical Atlantic for current and future climate conditions using the PGW approach
- We find an accurate representation of the annual cycle of shallow cumulus clouds and a realistic structure of the ITCZ, without double ITCZ
- The ITCZ intensifies in a warming climate while the narrowing typically seen in GCMs is not visible

Corresponding author: Christoph Heim, `christoph.heim@env.ethz.ch`

Abstract

Clouds over tropical oceans are an important factor in Earth's response to increased greenhouse gas concentrations, but their representation in climate models is challenging due to the small-scale nature of the involved convective processes.

We perform two 4-year-long simulations at kilometer-resolution (3.3 km horizontal grid spacing) with the limited-area model COSMO over the tropical Atlantic on a $9000 \times 7000\,\mathrm{km}^2$ domain: A control simulation under current climate conditions driven by the ERA5 reanalysis, and a climate change scenario simulation using the Pseudo-Global Warming (PGW) approach. We compare these results to the changes projected in the CMIP6 scenario ensemble.

We find a good representation of the annual cycle of albedo, in particular for trade-wind clouds, even compared to the ERA5 reanalysis. Also, the vertical structure and annual cycle of the marine intertropical convergence zone (ITCZ) is accurately simulated, and the simulation does not suffer from the double ITCZ problem commonly present in global climate models (GCMs). The ITCZ responds to warming through a vertical extension and intensification primarily at high levels, as well as a slight southward extension of the annual mean ITCZ, while the narrowing typically seen in GCMs is not visible.

1 Introduction

Clouds over tropical oceans are among the most uncertain factors controlling Earth's temperature response to anthropogenic greenhouse gas emissions (Forster et al., 2021). They form along the branches of the Hadley circulation (HC, e.g. Held & Hou, 1980), for instance, in the form of deep convection at the intertropical convergence zone (ITCZ) (Waliser & Gautier, 1993) and shallow convection in the marine boundary layer (MBL) in the Trades (e.g. Stevens, 2007; Wood, 2012; Vial et al., 2017). Tropical clouds have the potential for a strong radiative feedback in a warming climate (Bony & Dufresne, 2005; Zelinka et al., 2016). Yet, their evolution with climate change is uncertain (e.g. Bretherton, 2015), making them a prime focus of current climate change research.

Model intercomparison projects of global climate models (GCMs) such as the fifth or sixth phase of the Coupled Model Intercomparison Project (CMIP5, CMIP6, Taylor et al., 2012; Eyring et al., 2016) allow for an assessment of the magnitude and inter-model variability of cloud changes in a large ensemble of state-of-the-art GCMs. With respect to tropical deep convection at the ITCZ, many GCMs project that the upper part of the clouds (i.e. the anvils) will rise in a warming atmosphere and remain at approximately the same temperature, according to the fixed anvil temperature (FAT) hypothesis (Hartmann & Larson, 2002). As the anvils rise, they find themselves in a more stable environment which reduces the anvil cloud fraction according to the stability iris hypothesis (Bony et al., 2016). There is observational evidence supporting these hypotheses (Saint-Lu et al., 2020). High-resolution simulations in aqua-planet and slab-ocean configuration mostly reproduce this result of GCMs (Wing et al., 2020), even though there are exceptions (Satoh et al., 2012; Singh & O'Gorman, 2015; Ohno & Satoh, 2018).

GCMs also project a narrowing of the annual mean ITCZ with stronger convective ascent near the equator (Huang et al., 2013; Byrne & Schneider, 2016; Byrne et al., 2018), and a drying and widening of the subtropics, which together have been illustratively termed the "deep-tropics squeeze" (Lau & Kim, 2015). These projected changes of tropical deep-convection are statistically robust among GCMs (Lau & Kim, 2015), even though a non-negligible amount of models projects ITCZ changes of opposite sign (Byrne et al., 2018). Yet GCMs do not agree on the representation of the ITCZ under current climate conditions, for example, many models exert a double ITCZ structure (Mechoso et al., 1995; Zhang et al., 2019). While observations show one single annual mean marine ITCZ rain band north of the equator, many GCMs simulate an additional rain band south of the equator at certain locations and seasons. This so-called "double ITCZ problem" has existed for more than two decades (e.g. Fiedler et al., 2020) and is thought to be linked, among other factors, to air-sea interaction (e.g. Lin, 2007; Li & Xie, 2014) and aspects of convective parameterizations (e.g. Lin, 2007; Bellucci et al., 2010; Song & Zhang, 2018). The narrowing and intensification of the convective regions in the deep tropics in a warming climate found in GCMs is supported by observations (Wodzicki & Rapp, 2016; Byrne et al., 2018) and thermodynamic arguments (Jenney et al., 2020; Lau et al., 2020). However, it has been argued that the observed narrowing of the ITCZ refers to the width of the seasonal ITCZ band, while the deep-tropics squeeze is evident in the width of the annual-mean zonal-mean tropical ascent region (Zhou et al., 2020). No clear signal of a reduced mid-cloud fraction with warming was found in high-resolution simulations in aqua-planet configurations (Wing et al., 2020). Yet, aqua-planet configurations show a large degree of idealization compared to the real world. Comparably little is known about changes in the structure of the ITCZ from high-resolution climate simulations in real-world application (e.g. Satoh et al., 2012; Tsushima et al., 2014).

With respect to tropical low cloud changes, GCMs overall project a reduction of the low-cloud albedo, but the inter-model spread is much larger than in projections of deep convection (e.g. Zelinka et al., 2017; Vial et al., 2017). Also, there is a notorious negative cloud bias in subtropical low-cloud regions in GCMs (e.g. Noda & Satoh, 2014; Kawai & Shige, 2020). Large-eddy simulations (LES) show a more consistent climate change response of low clouds (e.g. Blossey et al., 2013), but given their small domain sizes and idealized setups, generalization of LES results to the entire planet introduces new uncertainties.

The fundamental problem behind the representation of convective clouds in GCMs is that a high horizontal and vertical resolution is required to resolve the small-scale convective circulations that drive clouds. Convective circulations represent the primary mode of vertical transport in the tropical atmosphere. If unresolved, these circulations, the clouds, as well as the vertical transport of heat and moisture associated with them have to be represented by convective parameterization schemes (e.g. Kawai & Shige, 2020). These schemes introduce substantial uncertainty in the simulation of deep-convective clouds (Suhas & Zhang, 2015), low-level clouds (Vial et al., 2016), and in how these clouds respond to climate change (Sherwood et al., 2014; Vial et al., 2017). With higher model resolution, convective parameterizations become less important and can eventually be switched off, which reduces the degree of parameterization and allows for a model formulation closer to physical first principles. For deep convective clouds, this threshold is reached at kilometer-resolution (Prein et al., 2015) which is why kilometer-resolution climate simulations are increasingly considered a major milestone towards more confident climate projections (e.g. Schneider et al., 2017; Satoh et al., 2019; Stevens et al., 2020; Schär et al., 2020). Precipitation statistics in the deep tropics have been found to be largely improved at kilometer-resolution compared to coarser models (Klocke et al., 2017; Stevens et al., 2020; Hohenegger et al., 2020).

Global kilometer-resolution multi-year climate simulations are not yet feasible due to computational cost (Schär et al., 2020), although rapid progress is evident (e.g. Satoh et al., 2012, 2019; Stevens et al., 2019). Instead, multi-year kilometer-resolution simulations are typically run on limited-area domains using boundary conditions from reanalysis data sets for evaluation runs (e.g. Ban et al., 2021), and from GCMs for climate change scenario simulations (e.g. Pichelli et al., 2021). Usually, a historical control simulation and a future scenario simulation are compared to extract the climate change signal. An alternative to this dynamical downscaling approach is the pseudo-global warming (PGW) approach (Adachi & Tomita, 2020; Brogli et al., 2022) in which reanalysis boundary conditions are used for both the control and the scenario simulation. The climate change signal is obtained by imposing large-scale changes in the climate system on the reanalysis boundary fields of the scenario simulation. Doing so has the advantage that the biases from the historical GCM run do not enter the limited-area simulation, and that relatively short simulation periods can be used (Brogli et al., 2022). The PGW approach has extensively been applied in the mid-latitudes (Schär et al., 1996; Wu & Lynch, 2000; Sato et al., 2007; Rasmussen et al., 2011; Kröner et al., 2017; Brogli et al., 2019). We are aware of applications in the subtropics (Chen et al., 2020; Nakamura & Mäll, 2021), but to our knowledge, this study represents the first application of a PGW simulation at kilometer-resolution covering the full extent of the HC including the deep tropics.

We run a 4-year-long limited-area atmospheric simulation at 3.3 km resolution over the tropical Atlantic with the goal to (i) evaluate how well the tropical climate and the associated distribution of clouds are represented in a kilometer-resolution atmospheric model, and (ii) compare the climate change response of the HC in terms of its structure, dynamics and clouds to the projections from the CMIP6 models. In a subsequent paper, a systematic analysis of the ensuing radiative feedbacks in this simulation will be presented. The following Section describes the modelling framework. Section 3 presents the results which are discussed in Section 4 and concluded in Section 5.

2 Materials and Methods

2.1 Experimental Setup

The limited-area model COSMO (see Section 2.3) is used in two 4-year-long simulations. The first one (CTRL) serves as a control simulation and represents current climate conditions. It is initialized and driven at the boundaries by the European Center for Medium Range Weather Forecast (ECMWF) ERA5 Re-Analysis (Hersbach et al., 2020). CTRL is used to evaluate the COSMO model against observations, and serves as a baseline for comparison with the second simulation. The second simulation is a cli-

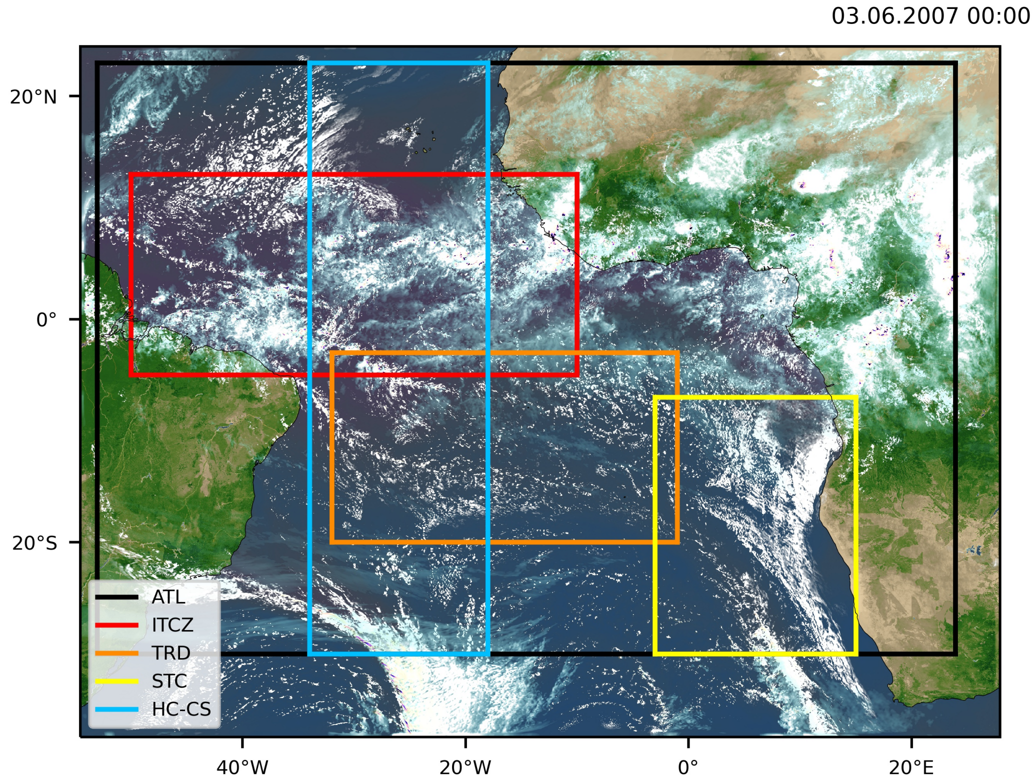

Figure 1. Simulation visualization and analysis domains. The COSMO simulations are run on the entire domain shown and the rectangles indicate different analysis domains. ATL covers the South Atlantic deep tropics and subtropics (30°S-23°N). The three subdomains ITCZ, TRD and STC comprise the regions of the three major tropical marine cloud regimes (deep convection at the ITCZ, trade-wind cumulus and stratocumulus). The HC-CS is used to compute altitude-latitude cross-sections to visualize the structure of the Hadley cell.

mate change scenario simulation (PGW) obtained with the pseudo-global warming approach (see Section 2.2).

Both, CTRL and PGW simulations are initialized on August 1, 2006 (for details on the initialization see below) and the analysis is done for the years 2007-2010 and focused on five geographic regions (Fig. 1). The analysis period is too short to fully average out inter-annual variability. The effect of this is quantified in Section 3. The simulation domain covers 37.5° S - 24.5° N and 54.5° W - 28.0° E and consists of 2750 x 2065 x 60 grid points at 0.03° / 3.3 km resolution, integrated with a time step of 25 seconds. The vertical grid stretches to an altitude of 30 km with a resolution of about 20 m near the surface, 500 m at 5 km altitude, and 1.5 km at the model top. The domain covers the deep-tropical and parts of the subtropical Atlantic (Fig. 1) encompassing the full southern hemispheric branch of the HC. Although the focus lies on the Atlantic, the simulation domain includes parts of Africa and South America to enable interaction between marine and continental areas for instance through Monsoon circulations or the African easterly waves.

2.2 Pseudo-Global Warming Approach

The initial and boundary conditions of the PGW simulation are obtained following Brogli et al. (2022) by adding the mean climate change signal (so-called climate deltas) for temperature, relative humidity, horizontal wind, and surface temperature to the ERA5 boundary conditions of the CTRL simulation period. The climate deltas are a function of latitude, longitude, pressure and month, and represent the mean annual cycle of the spatial change pattern between two climate states, i.e. here between a historical and a future scenario climatology. Note that, apart from the model initialization, the climate deltas are only applied at the lateral boundary conditions of the limited-area model, and at the surface for SST. The change signal PGW−CTRL in the interior of the domain is thus a model-internal response to the forcing applied at the boundaries.

The climate deltas are computed from the CMIP6 output of the MPI-ESM1-2-HR model (von Storch et al., 2017) as the difference between the Intergovernmental Panel on Climate Change (IPCC) SSP5-8.5 scenario (Kriegler et al., 2017) simulation during 2070 - 2099 and the CMIP6 historical simulation during 1985 - 2014. The output of the MPI-ESM is obtained as daily mean values from the CMIP6 output group CFday and aggregated into monthly means. Since this output group was intended for the Cloud Feedback Model Intercomparison Project (Webb et al., 2017) it is provided on the native vertical grid of the MPI-ESM model, and hence at fine vertical resolution. Fine resolution is desirable to accurately represent the difference in warming across the trade-wind inversion (see Brogli et al., 2022, Fig. 4 and corresponding discussion). The obtained changes are displayed in the supplemental information (Figs. S1-4).

The monthly mean climate deltas are then linearly interpolated to the grid and time of the ERA5 boundary files of the CTRL simulation where the deltas are added to obtain the boundary files of the PGW simulation. After modifying temperature and relative humidity, the pressure field is adjusted to restore the hydrostatic balance. The corresponding changes in cloud and precipitation quickly adjust to the new thermodynamic environment within the model domain, and are thus not otherwise accounted for in the PGW methodology. The change of the soil temperature is computed based on the surface temperature climate delta assuming an exponential decay of the annual cycle signal with depth. Initial soil moisture is not modified and taken from the CTRL simulation (5 months before the analysis period begins). Greenhouse gas concentrations are held fixed during the simulation and set to 530 ppm CO_2-eq during CTRL and 1100 ppm CO_2-eq during PGW consistent with the SSP5-8.5 scenario. Aerosols are identical in CTRL and PGW following the Tegen et al. (1997) climatology. Even though biomass burning over Africa is a significant source of aerosol over the Atlantic (Zuidema et al., 2016), the change of aerosol loading between CTRL and PGW is neglected here for simplicity. The same is the case for ozone.

2.3 COSMO Model

The COSMO model is a fully compressible non-hydrostatic atmospheric model originally developed as a numerical weather prediction model (Baldauf et al., 2011) and later evolved into a regional climate model (Rockel et al., 2008). Here a COSMO version capable of exploiting Graphics Processing Units is employed (Fuhrer et al., 2014; Leutwyler et al., 2016). This version of COSMO has been extensively validated in kilometre-scale configurations including a 10-year-long reanalysis-driven simulation over Europe (Leutwyler et al., 2017), validation of clouds (Hentgen et al., 2019), and surface winds (Belušić et al., 2018). The model discretizes the horizontal and vertical dimensions on a rotated latitude-longitude grid and a generalised Gal-Chen coordinate, respectively. The model equations are integrated in time with a split-explicit third-order Runge-Kutta scheme (Klemp &

Wilhelmson, 1978; Wicker & Skamarock, 2002; Baldauf et al., 2011). Horizontal advection is treated with a fifth-order advection scheme except for moist quantities which are integrated using a positive-definite second-order scheme (Bott, 1989). The upper boundary is treated following (Klemp & Durran, 1983) and no relaxation of the model top towards the boundary files is performed.

Radiative transfer is computed following the δ-two-stream approach after Ritter and Geleyn (1992). The subgrid-scale vertical turbulent fluxes are parameterized with a TKE-based model (Raschendorfer, 2001). Cloud microphysics is parameterized using the single-moment bulk scheme after Reinhardt and Seifert (2006). The parameterizations for deep and shallow convection are switched off as this was previously found to give a reasonable representation of clouds in the COSMO model at kilometer-resolution (Vergara-Temprado et al., 2020; Heim et al., 2021). At the surface, the second-generation land-surface model TERRA_ML (Heise et al., 2003) with the groundwater-runoff scheme after Schlemmer et al. (2018) is used on land grid points.

Soil moisture profiles are initialised based on a 12-year-long soil spin up COSMO simulation at 24 km grid spacing. The resulting soil moisture conditions serve as initial condition for a 5-month-long spin up at full (3.3 km) resolution, initialized on August 1, 2006 (for CTRL and PGW). Over ocean grid points, sea-surface temperature is read in from the surface boundary fields. Lateral and surface boundary fields are updated every three hours. A number of empirical model parameters are adjusted to improve the representation of low clouds in comparison to previous simulations over the extratropics: The vertical turbulent length scale is set to 200 m. The minimum threshold for eddy-diffusivity for heat and momentum under stable conditions are set to $0.25\,\mathrm{m^2\,s^{-1}}$ (see Possner et al. (2014) for more details about these parameters).

2.4 Data Sources

2.4.1 CMIP6 Models

The change signal between the future and the historical climate in COSMO is obtained by taking the difference between the PGW and the CTRL simulation. To put this into perspective, the change signal of the ensemble mean of 26 CMIP6 models[1], hereafter referred to as CMIP6-EM, is computed as the difference between the SSP5-8.5 experiment during 2070-2099 (SCEN), and the historical experiment during 1985-2014 (HIST). SCEN−HIST is thus consistent with (and in the case of the MPI-ESM model equivalent to) the climate delta of the PGW simulation. The CMIP6-EM is computed using output of the Amon group, thus with monthly frequency and on 11 pressure levels below 100 hPa. One exception is the cloud fraction which is provided on the native vertical grid. All analyses are performed in geometric altitude space, and the CMIP6 data is vertically interpolated on a z-coordinate.

2.4.2 Observational Data Sets

The following observational data sets are used to evaluate the simulations:

- The Clouds and the Earth's Radiant Energy System (CERES) Energy Balanced and Filled (EBAF) Top-of-Atmosphere (TOA) Edition-4.0 Data Product (Loeb et al., 2018) provides monthly values of TOA radiation at 1° horizontal resolution.
- The Satellite Application Facility on Climate Monitoring (CM SAF) TOA radiation (Clerbaux et al., 2013), based on the Geostationary Earth Radiation Budget (GERB) instrument, provides monthly values of TOA radiation at 45 km horizontal resolution.
- The global Precipitation Measurement (GPM) Integrated Multi-satellitE Retrievals for GPM (IMERG) data set (Huffman et al., 2019): provides precipitation observations at daily frequency and 0.1° horizontal resolution.
- The ERA5 reanalysis (Hersbach et al., 2020) is a gridded reanalysis data set. It is obtained from the CDS data store (Copernicus Climate Change Service (C3S), 2017) and used at 3-hourly frequency and 0.25° horizontal resolution.

[1]

[1] The analysed models include: ACCESS-CM2, ACCESS-ESM1-5, CAMS-CSM1-0, CanESM5, CESM2, CESM2-WACCM, CMCC-CM2-SR5, CMCC-ESM2, CNRM-CM6-1, CNRM-ESM2-1, E3SM-1-1, FGOALS-f3-L, FGOALS-g3, GFDL-CM4, GFDL-ESM4, GISS-E2-1-G, HadGEM3-GC31-LL, MIROC6, MIROC-ES2L, MPI-ESM1-2-HR, MPI-ESM1-2-LR, MRI-ESM2-0, NorESM2-LM, NorESM2-MM, TaiESM1, UKESM1-0-LL

3 Results

We start by looking at a cloud visualization to provide an overview of the cloud phenomena occurring within the domain. Figure 2 shows snapshots during boreal summer (top) and winter (bottom). The variety of shapes and scales of tropical cloud phenomena and their representation in the model is remarkable. We list some of the key phenomena in order of decreasing size and show close-up views of them in the small panels (i)-(vi): (i) A mid-latitude frontal system moving eastward across the southern subtropical Atlantic. Such extra-tropical disturbances can reach far into the southern Atlantic subtropics during boreal summer and alter the properties of the atmosphere and subsequent formation of MBL clouds (e.g. Schulz et al., 2021). (ii) to the North of the domain, a tropical cyclone with multiple rain bands has formed and makes its way towards north-west. (iii) Large mesoscale convective systems travelling westward are producing heavy rainfall over the African tropical belt. (iv) Deep convection at the marine ITCZ. (v) The vast region of the Namibian stratocumulus decks (visible in both panels, but with larger extent during boreal winter). Finally, the stratocumulus topped MBL transitioning into (vi) the trade-wind-cumulus topped MBL on its way towards the deep tropics. Hereby, different modes of mesoscale cloud aggregation are producing regional differences in cloud cover.

The horizontal and vertical circulations underlying the clouds shown in Fig. 2 – from the large-scale tropical overturning HC down to small-scale convective MBL circulations – are all represented explicitly on the model grid, even though many of the circulation features are resolved only at the coarse end of the spectrum. In the following section, we are going to evaluate the simulation and compare it to the CMIP6 historical runs.

3.1 Evaluation of the CTRL Simulation

We start the evaluation at the large-scale with the analysis of the meridional structure of the HC. Afterwards, we look at the spatial structure and annual cycle of individual cloud regimes.

3.1.1 The Hadley Cell

Figure 3 shows the meridional distribution of clouds and surface precipitation along the HC-CS domain for the annual mean as well as for the 3-month-periods with south-

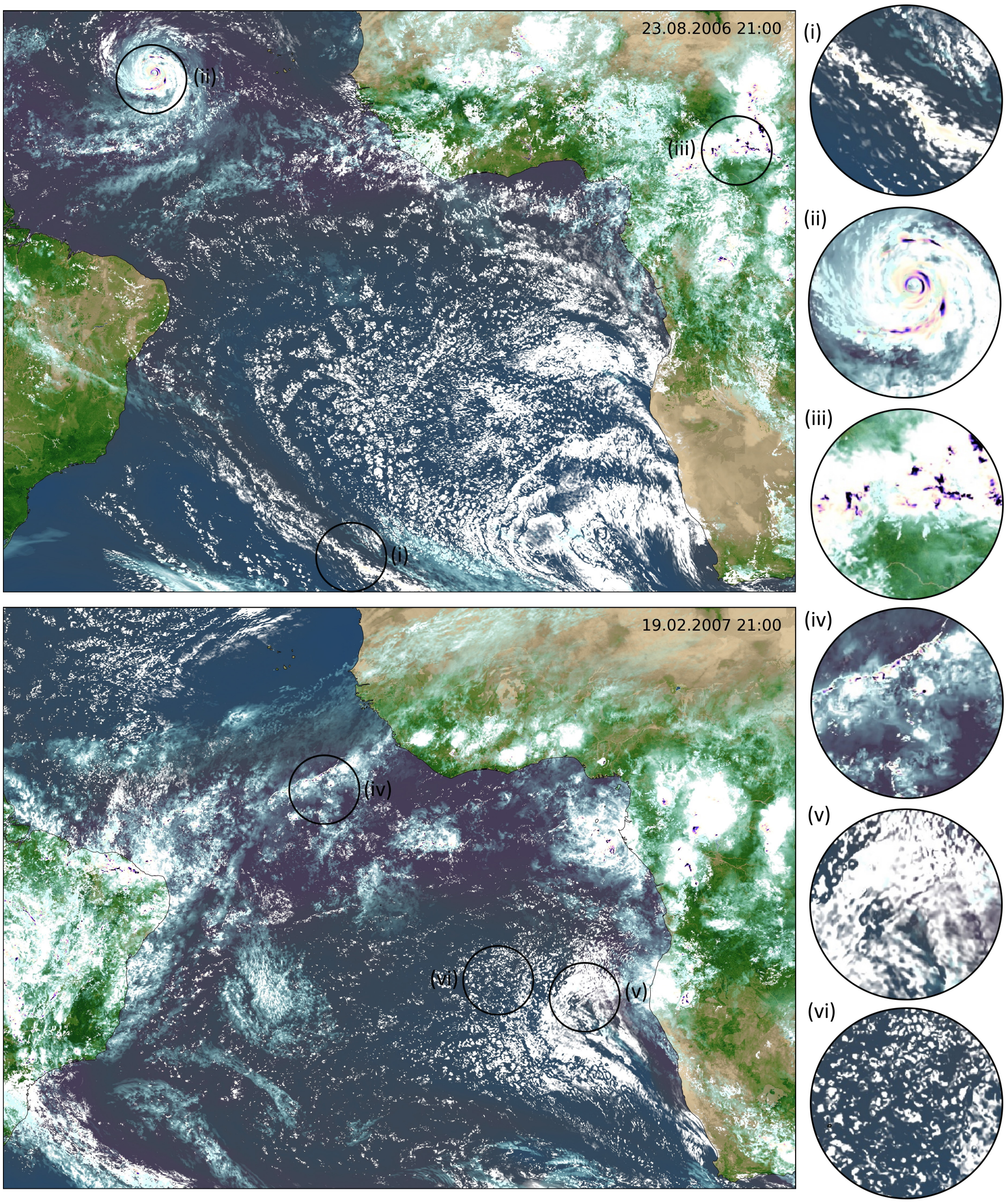

Figure 2. Snapshots of the CTRL simulation obtained during boreal summer on 23.08.2006 21:00 UTC (top) and winter on 19.02.2007 21:00 UTC (bottom). The visualization shows atmospheric cloud liquid and ice water content in white and light-blue-to-white colors, respectively, as well as surface precipitation in yellow-to-blue colors. Areas of high atmospheric water vapor content over oceans are visualized using purple shading. The land surface is rendered based on the model surface albedo and vegetation types, with a desert-to-green color gradient that is modulated by the soil moisture content to imitate the seasonal cycle of vegetation density. The panels on the right-hand side show close-up views of (i) a mid-latitude frontal system, (ii) a tropical cyclone, (iii) a mesoscale convective system, (iv) deep convection at the marine ITCZ, (v) marine stratocumulus clouds, (vi) marine shallow cumulus (or trade-wind cumulus) clouds. An animation of this visualization can be obtained via `https://doi.org/10.3929/ethz-b-000568941`.

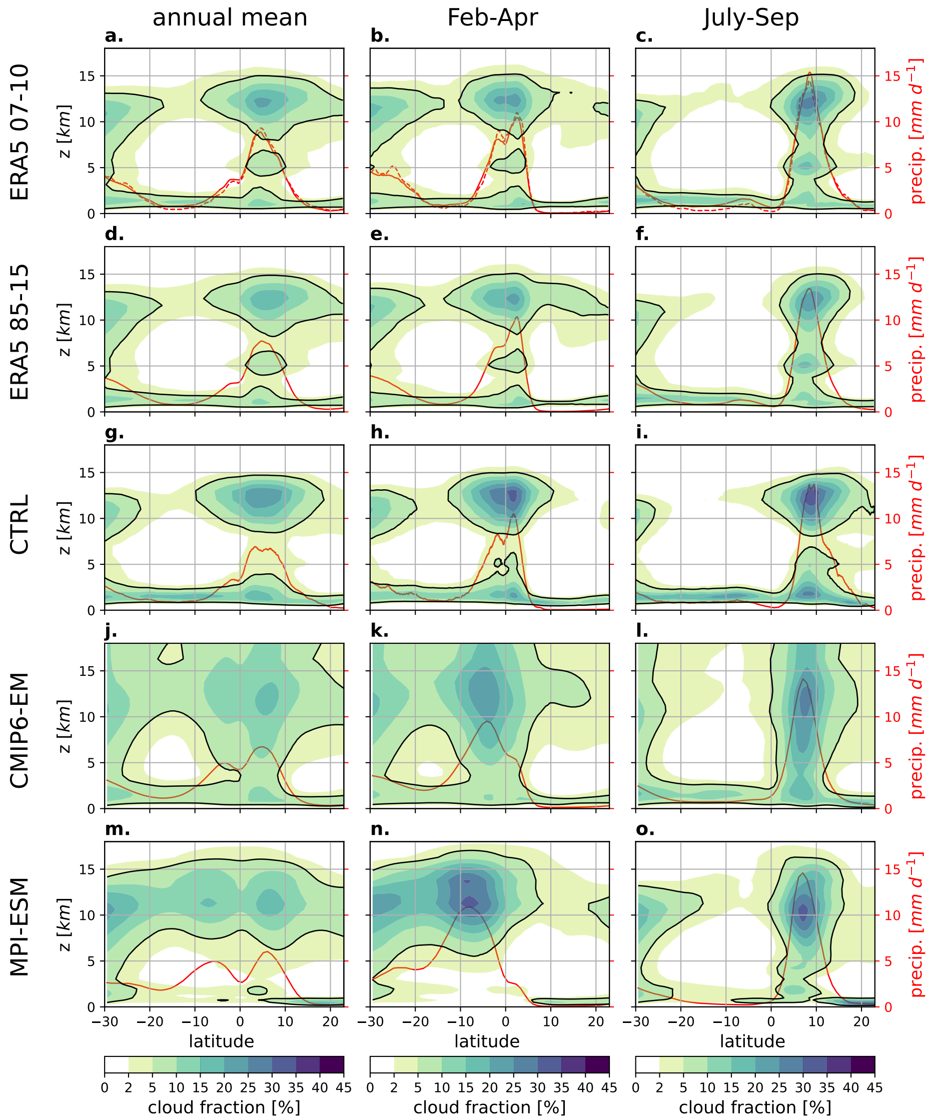

Figure 3. Altitude-latitude cross-sections of the cloud fraction [%] averaged along the longitudes of the HC-CS domain. The black contour lines denote the 5% cloud fraction level. The solid red lines show surface precipitation [$\mathrm{mm\,d^{-1}}$]. The corresponding y-axis is located on the right-hand side of the panels. The panels show (a-c) ERA5 with the same period as the CTRL simulation (2007-2010), (d-f) an extended period of ERA5 corresponding to HIST (1985-2014), (g-i) CTRL (2007-2010), (j-l) CMIP6-EM HIST (1985-2014), and (m-o) MPI-ESM HIST (1985-2014). The three columns represent multi-year averages (left panels) during the entire year, as well as (center panels) during February–April and (right panels) July–September when the marine ITCZ reaches its southernmost and northernmost extent, respectively. The cloud fraction is obtained from the respective model output, except for COSMO where grid points with a specific cloud liquid plus ice water content $\geq 0.01\,\mathrm{g\,m^{-3}}$ are considered cloudy while the remaining grid points are considered cloud-free. As a complementary reference observation, GPM IMERG precipitation is shown as a red dashed line in panels (a-c).

ernmost (February-April) and northernmost (July-September) extent of the marine ITCZ. The ERA5 record (Fig. 3a-c) indicates that the annual mean cloud fraction and precipitation have their peak at 4°N. The peak shifts to 8°N during boreal summer, and splits into a primary peak persisting at 3°N, and a secondary peak at about 2°S during boreal winter. Comparing the 4-year-long (Fig. 3a-c) and the 30-year-long (Fig. 3d-f) ERA5 cross-sections shows that the climatological distributions of cloud and precipitation are well represented by the 4-year-long simulation period used in CTRL (see Section 2.1). The comparison of surface precipitation between ERA5 and GPM IMERG indicates a close agreement between these two reference data sets (Fig. 3a-c).

The zonal mean precipitation is well reproduced in CTRL with respect to ERA5 with the exception of a slightly underestimated annual mean peak (Fig. 3g-i). The CMIP6-EM captures the northward shift of the ITCZ during boreal summer, but largely overestimates the boreal winter secondary peak in the southern hemisphere (Fig. 3j-l). The latter is a manifestation of the double ITCZ problem (Fig. 3j). Besides an overestimation of precipitation and clouds in the southern hemispheric deep tropics, the double ITCZ also results in too frequent subtropical high clouds. We further show the cross-sections for the MPI-ESM model individually (Fig. 3m-o), as it is used to compute the climate delta for the PGW simulation. The double ITCZ problem is more pronounced in the MPI-ESM model than in the CMIP6-EM and results in a bimodial annual mean precipitation distribution that is almost symmetric about the equator.

In ERA5, the cloud field at the ITCZ consists of (i) a concentration of low-level clouds, (ii) a secondary liquid cloud maximum at around 5 km (which appears to be related to an elevated inversion layer), and (iii) the deep-convective anvil clouds between 8-15 km altitude. In the subtropics, the free troposphere contains virtually no clouds below 10 km as a result of the stable and dry conditions in the downward branch of the HC. At the surface, low clouds are topping the MBL. The MBL is less shallow south of the equator than north of the equator. In the former case, the MBL is located further off the coastal upwelling regions of Africa, and thus experiences warmer sea surface temperature (SST) favoring the development of a deep MBL (e.g. Bretherton & Wyant, 1997). Beyond 25°S, clouds of extra-tropical origin penetrate into the subtropical atmosphere, in particular at high altitudes, where they contribute to the subtropical high-cloud fraction.

The annual mean and seasonal structure of ITCZ clouds in CTRL corresponds well with ERA5 (Fig. 3a-c,g-i). The main difference is that in the annual mean and during Feb-Apr, the extra-tropical clouds reach less far into the subtropics in CTRL. Overall, the differences are not fundamental and we conclude that CTRL simulates the cloud field along the HC consistent with ERA5. In contrast, the CMIP6-EM does not reproduce the vertical cloud structure at the ITCZ as seen in ERA5 and CTRL (Fig. 3d-f,j-l). Instead, many of the analysed CMIP6 members simulate a too coherent cloud field throughout the tropical tropospheric column which also penetrates too high up into the tropical tropopause layer in some models. Although the focus of this study lies on marine clouds, the structure of the HC over land is shown in supplementary Fig. S6. While the vertical cloud structure in CTRL is comparable to ERA5, the high-cloud fraction and surface precipitation is significantly larger than in ERA5 and GPM IMERG. These quantities are both related to deep convection and thus indicate that deep convection at the continental ITCZ may be overestimated in CTRL, as will be shown later.

The first two columns of Fig. 4 show the large-scale overturning motion of the HC in terms of the meridional and vertical mass flux along the HC-CS domain. Air rises at the surface of the ITCZ and diverges above an altitude of 10 km towards the poles. The poleward (i.e., the elevated) branch of the HC converges with the northward branch of the Ferrel cell at 15°S in ERA5 (Fig. 4a) which sets the latitude of strongest subtropical subsidence (Fig. 4b). The HC is closed by the trade winds at the surface that are largely confined to the MBL and converge at 5°N (Fig. 4a).

Compared to ERA5, the poleward branch of the HC in the southern hemisphere reaches further south in CTRL and the CMIP6-EM (Fig. 4a,e,i). Consequently, the subtropical subsidence extends further south in CTRL and the CMIP-EM than in ERA5 (Fig. 4b,f,j). This dynamical difference between CTRL and ERA5 is consistent with the differences in the high-cloud fraction of extra-tropical origin at around 20°S between CTRL and ERA5 (Fig. 3a,g). A further difference between CTRL and ERA5 is related to the ITCZ outflow in the lower troposphere. ERA5 shows a pronounced shallow circulation between 2 km $<$ z $<$ 6 km (Fig. 4a) which is much weaker in CTRL (Fig. 4e). Thus, while the HC in ERA5 has a pronounced dual circulation structure (i.e. a deep circulation and a shallow circulation), the shallow circulation is almost absent in CTRL and the deep circulation is stronger (Fig. 4m). In line with that, the subtropical subsidence profile in ERA5 shows a pronounced maximum at 3 km (Fig. 4b), while it is more constant through-

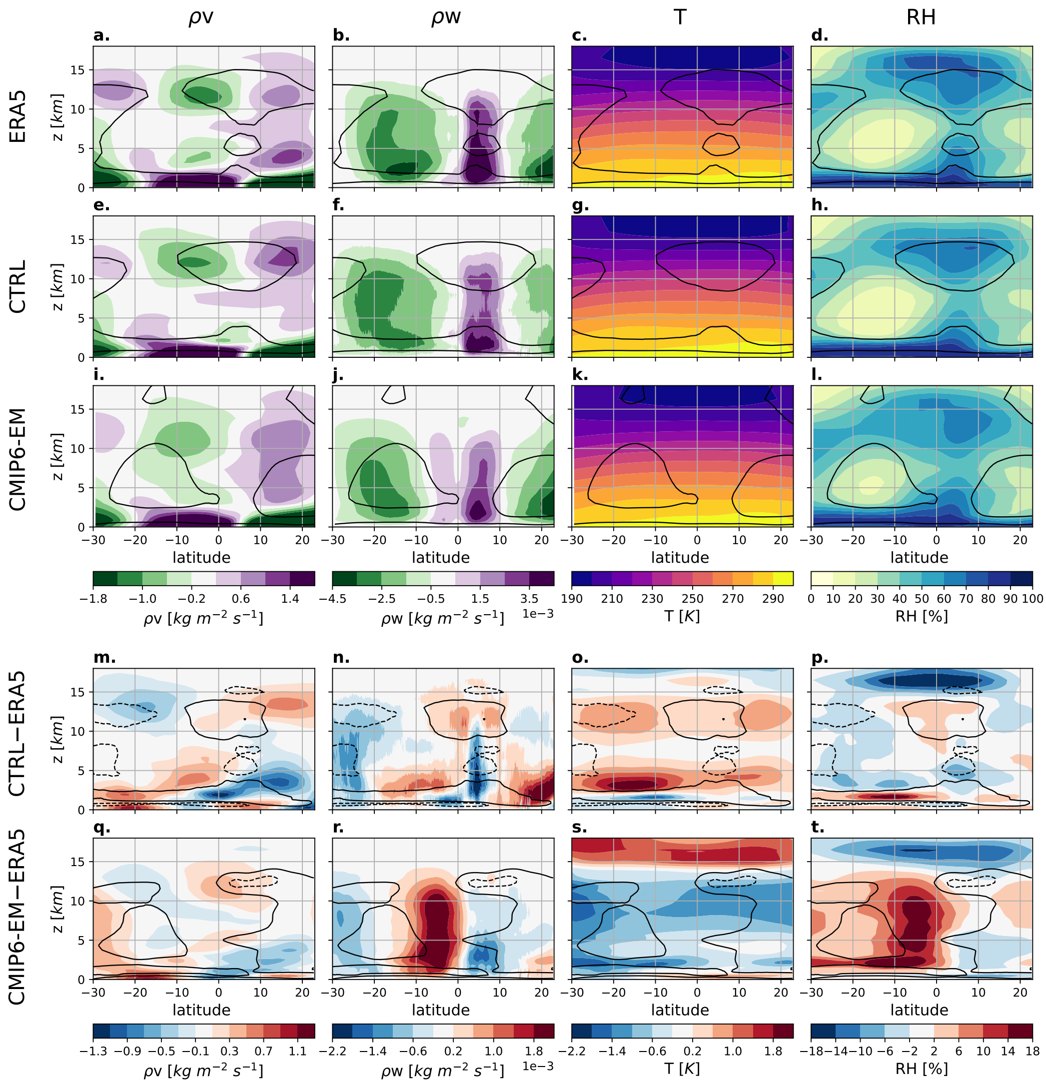

Figure 4. Annual mean altitude-latitude cross-sections of (first column) meridional mass flux [kg m^{-2} s^{-1}], (second column) vertical mass flux [kg m^{-2} s^{-1}], (third column) temperature [K], and (fourth column) relative humidity [%] averaged along the longitudes of the HC-CS domain. The panels show (a-d) ERA5 (2007-2010), (e-h) CTRL (2007-2010), (i-l) CMIP6-EM HIST (1985-2014), and the difference between (m-p) CTRL and ERA5 (2007-2010), and (q-t) CMIP6-EM HIST and ERA5 (1985-2014). The black contour lines indicate (a-l) the 5% cloud fraction level and (m-t) the 2% level of difference in the cloud fraction level where solid (dashed) lines represent a positive (negative) difference.

out the troposphere in CTRL (Fig. 4f). Differences in subsidence can result from differences in the radiative cooling rate or temperature stratification. The weaker subtropical subsidence at low levels in CTRL appears to be due to weaker radiative cooling rate compared to ERA5 (see supplementary Fig. S7). The meridional outflow of the ITCZ in the CMIP6-EM (Fig. 4i) is more evenly distributed over the free-tropospheric column compared to CTRL and ERA5, in line with the evenly distributed cloud fraction (Fig. 3j-l). Further, the imprint of the double ITCZ is well visible in the bias of the vertical wind field, showing an anomalous upward motion south of the equator compared to ERA5 (Fig. 4r).

The third and fourth columns of Fig. 4 show the thermodynamic structure of the HC along the HC-CS domain. Temperature in CTRL does not deviate from ERA5 by more than 1 K except in the subtropical lower troposphere (Fig. 4o). The differences in relative humidity between CTRL and ERA5 (Fig. 4p) are also small except for altitudes above 15 km where temperatures are very low and small differences in the amount of deep-convective outflow have a large effect on the relative humidity. Overall, the subtropical troposphere is slightly drier in CTRL than in ERA5, and (as for temperature) the differences are largest in the lower troposphere. The trade-wind inversion in CTRL is more elevated than in ERA5 which explains the lower temperature and enhanced humidity in CTRL in between (i.e. between 1-2 km). Above the inversion, the differences may be related to lower-tropospheric mixing which alters the moisture content of the free troposphere and thus modulates the clear-sky radiative cooling rate. The drier free troposphere in CTRL (Fig. 4p) may thus explain the weaker radiative cooling rate at these levels (Fig. S7), and consequently the warmer temperature (Fig. 4o) and weaker subsidence (Fig. 4n) in the subtropical lower troposphere in CTRL. The biases in temperature and relative humidity in the CMIP6-EM (Fig. 4s,t) are larger than in CTRL. This is expected since CTRL is driven by ERA5 at its boundaries while the CMIP6 simulations are global. Tropospheric temperature is lower in the CMIP6-EM than in ERA5 while stratospheric temperature is higher (Fig. 4s). Further, the deep tropics in the southern hemisphere are much moister than in ERA5, due to the double ITCZ (Fig. 4t).

3.1.2 Tropical Cloud Regimes

We continue with a more detailed evaluation of clouds and precipitation. Figure 5 shows the annual mean spatial pattern of the TOA albedo, surface precipitation, and TOA OLR. The low-cloud albedo is substantially overestimated in CTRL (Fig. 5c). Surface

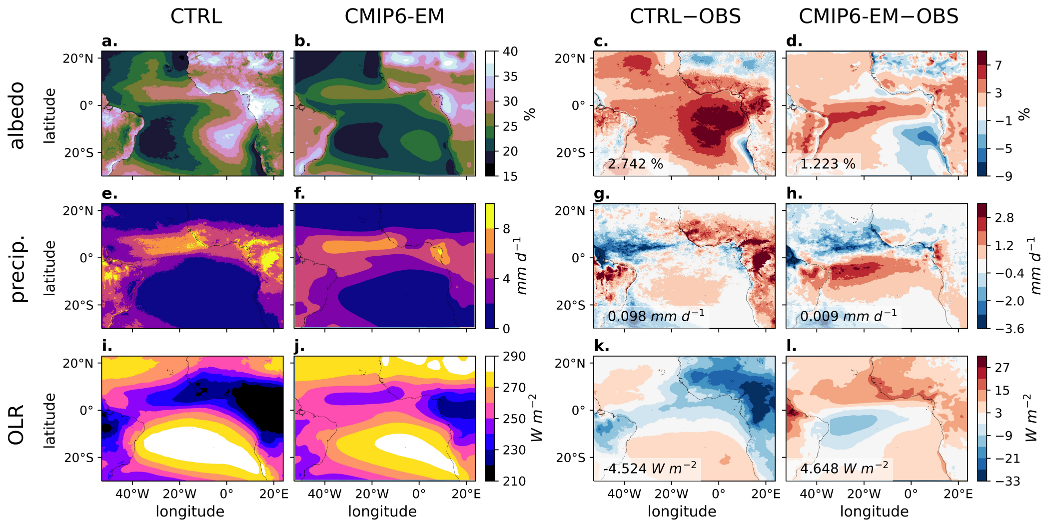

Figure 5. Evaluation of (a-d) TOA albedo [%], (e-h) surface precipitation [mm d^{-1}], and (i-l) TOA outgoing longwave radiation (OLR) [W m^{-2}]. The panels show (first coulumn) CTRL (2007-2010), (second column) CMIP6-EM HIST (1985-2014), (third column) CTRL - OBS (2007-2010), and (fourth column) CMIP6-EM HIST (1985-2014) - OBS, where OBS is (c,d,k,l) the CM SAF record during (c,k) 2007-2010 and (d,l) 2004-2010, and (g,h) the GPM IMERG record during (g) 2007-2010 and (h) 2001-2014. The comparison between the CMIP6-EM and the OBS is thus based on the longest available observational period overlapping with HIST. The labels in the lower-left corners show domain average biases.

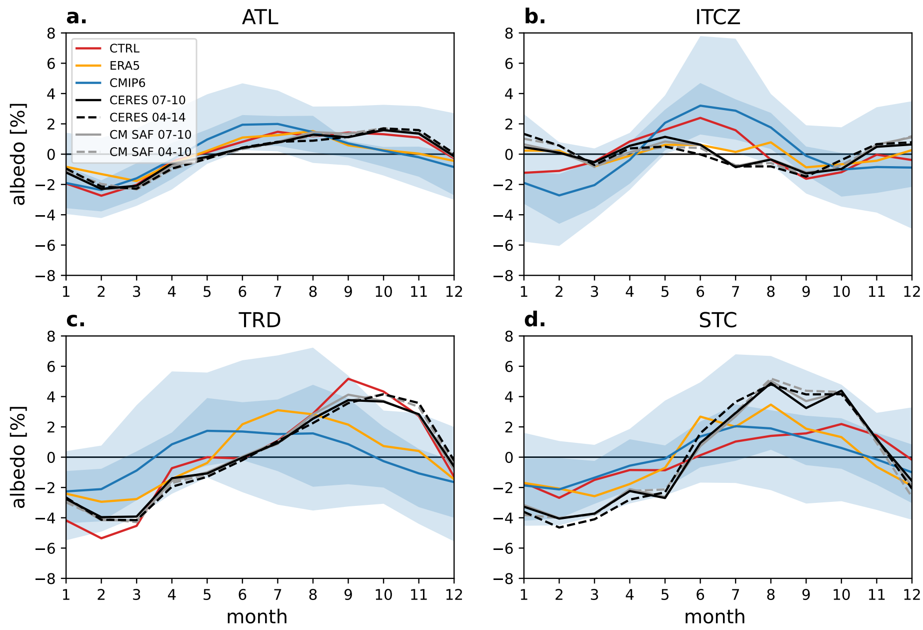

Figure 6. Evaluation of the mean annual cycle of TOA albedo shown for the four marine analysis domains (a) ATL, (b) ITCZ, (c) TRD and (d) STC. The annual cycle, expressed as the deviation from the annual mean, is shown for CTRL (2007-2010, red), ERA5 (2007-2010, yellow), CMIP6-EM HIST (1985-2014, blue), CERES EBAF (2007-2010, solid black), CERES EBAF (2004-2014, dashed black), CM SAF (2007-2010, solid gray), and CM SAF (2004-2010, dashed gray). The shading shows the CMIP6 ensemble spread between the 10th and 90th percentile (light blue) and the interquartile range (dark blue). Only ocean grid points are used in this figure.

precipitation in CTRL is overestimated over land in comparison to the GPM IMERG data set (Fig. 5g). The precipitation of the marine ITCZ is well represented to the East, but its westward extent is underestimated. OLR is far too low over land (Fig. 5k), in line with the precipitation bias. Over sea, the underestimation of OLR in the deep tropics is smaller, but subtropical OLR is overestimated. The CMIP6-EM bias patterns of these three variables (Fig. 5d,h,l) reveal the two well-known deficits of GCMs over low-latitude oceans: The double ITCZ problem and the underestimation of stratocumulus clouds. Also note that over land, the CMIP6-EM shows much smaller biases than CTRL.

We continue with the evaluation of the annual cycle of clouds on the four marine analysis domains ATL, ITCZ, TRD and STC. Figure 6 shows the mean annual cycle of TOA albedo in CERES EBAF, CM SAF, CTRL, ERA5, and the CMIP6 mean and en-

Table 1. Domain and time average values of TOA albedo [%], precipitation [mm d^{-1}] and OLR [W m^{-2}] on the four marine analysis domains ATL, ITCZ, TRD and STC shown for CTRL (2007-2010), ERA5 (2007-2010), CMIP6-EM HIST (1985-2014) and the satellite observations (CERES EBAF and CM SAF for albedo and OLR, and GPM IMERG for precipitation). As in Figs. 6-8, the satellite observations are listed during the CTRL period (2007-2010) and during the longest period overlapping with the HIST period (2004-2014 for CERES EBAF, 2004-2010 for CM SAF, and 2001-2014 for GPM IMERG).

albedo. [%]	ATL	ITCZ	TRD	STC
CTRL	24.5	24.5	23.8	27.7
ERA5	21.5	22.0	20.1	21.6
CMIP6-EM	22.2	23.1	20.6	22.2
CERES EBAF 07-10	21.1	21.4	18.8	24.4
CERES EBAF 04-14	21.2	21.3	18.8	24.7
CM SAF 07-10	20.9	20.9	18.8	24.5
CM SAF 04-10	21.0	21.0	18.9	24.9

precip. [mm d^{-1}]	ATL	ITCZ	TRD	STC
CTRL	2.10	4.15	0.95	0.37
ERA5	2.45	5.12	0.91	0.30
CMIP6-EM	2.46	4.58	1.72	0.52
GPM IMERG 07-10	2.44	5.01	0.57	0.20
GPM IMERG 01-14	2.33	4.78	0.49	0.19

OLR [W m^{-2}]	ATL	ITCZ	TRD	STC
CTRL	262.4	248.0	280.4	274.4
ERA5	269.5	259.4	285.0	279.3
CMIP6-EM	264.2	255.4	273.9	275.8
CERES EBAF 07-10	267.4	255.6	283.7	277.3
CERES EBAF 04-14	267.7	256.4	284.2	277.5
CM SAF 07-10	261.3	250.5	277.2	269.7
CM SAF 04-10	261.5	251.0	277.8	270.0

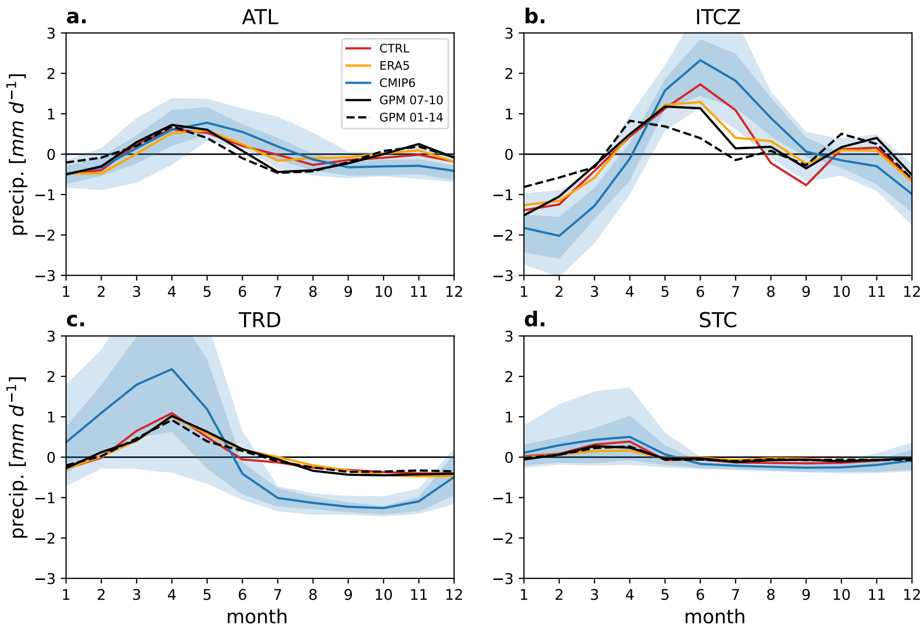

Figure 7. As Fig. 6 but showing surface precipitation. The black lines show GPM IMERG (2007-2010, solid) and GPM IMERG (2001-2014, dashed).

semble spread. The annual cycle is expressed as deviations from the annual mean. Table 1 lists the annual mean values for all data sets and analysis domains. Both observational records (CERES EBAF in black and CM SAF in grey) show very similar results for albedo, and are shown during the CTRL period (2007-2010, solid lines), but also during the longest available period overlapping with HIST (i.e. 2004-2014 and 2004-2010, dashed lines) to assess the effect of inter-annual variability. The annual cycle of the 4-year-period is very similar as in the extended period, indicating that the former is representative of the long-term conditions. Table 1 shows that the marine albedo in CTRL is overestimated by approximately 3.5%. However, the timings of annual maximum and minimum cloud cover as well as the amplitude of the annual cycle are much improved in CTRL compared to the CMIP6-EM on the ATL (Fig. 6a) and the TRD (Fig. 6c) domains, where CTRL even outperforms the ERA5 record. On the ITCZ (Fig. 6b) and the STC (Fig. 6d) domains, on the other hand, similar (though mitigated) deficiencies as in the CMIP6-EM are visible, i.e., an overestimation and underestimation of the ITCZ albedo during boreal summer and winter, respectively, as well as an underestimation of the annual cycle on the STC domain.

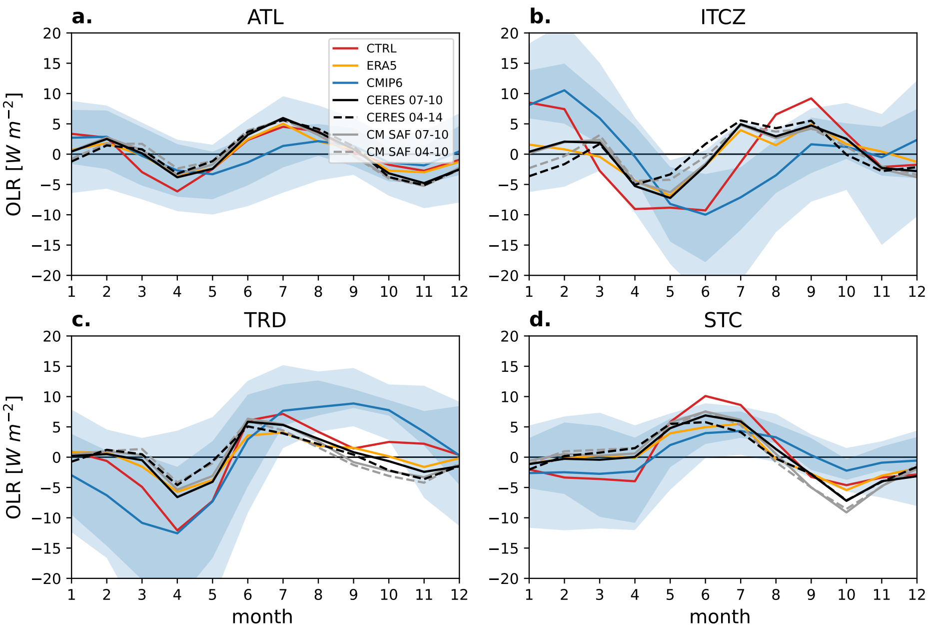

Figure 8. As Fig. 6 but showing TOA outgoing longwave radiation (OLR).

Figure 7 shows the annual cycle of surface precipitation over the marine analysis domains. The annual cycle is overall well represented in CTRL with the largest deviations found over the ITCZ domain (Fig. 7b), where the simulated timing of maximum precipitation lags one month behind the observed due to an overestimation of the boreal summer precipitation (similar as for the albedo in Fig. 6). The relative difference in precipitation amount between the different domains is well simulated in CTRL, but with slightly more precipitation on the TRD and the STC domains compared to GPM IMERG (Table 1). In the CMIP6-EM, the precipitation amount over the TRD is overestimated more strongly due to the double ITCZ problem.

The annual cycle of OLR is shown in Fig. 8. Unlike for the albedo, there is a surprisingly large difference between CERES EBAF and CM SAF of about 6 $\mathrm{W\,m^{-2}}$ (Table 1). ERA5 is closer to CERES EBAF. The amplitude of the annual cycle of OLR in CTRL is overestimated on the three small analysis domains (ITCZ, TRD and STC; Fig. 8b-d). This appears to be mainly due to an overestimated high-cloud fraction originating at the ITCZ during the first half of the year and resulting in too much downwelling longwave radiation. We further see a signal of too high tropospheric water vapor content (not shown) originating from the African ITCZ which contributes to the opacity of the at-

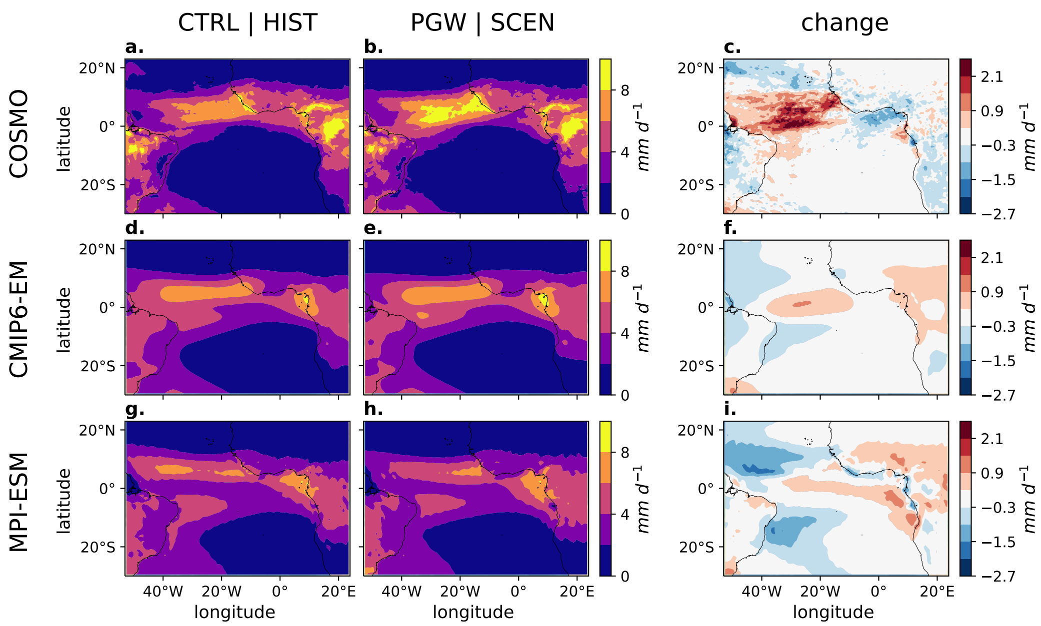

Figure 9. Annual mean climate-change signal of mean surface precipitation [mm d^{-1}]. The panels show (a-c) CTRL (2007-2010) and PGW (2007-2010), (d-f) the CMIP6-EM for HIST (1985-2014) and SCEN (2070-2099), and (g-i) the MPI-ESM model for HIST and SCEN. The columns show the simulated precipitation during (first column) CTRL and HIST, (second column) PGW and SCEN, and (third column) the change between CTRL and PGW, and between HIST and SCEN, respectively. CTRL and PGW are remapped to a 50 km grid.

mosphere over the Atlantic. Similar as for precipitation, the error of CTRL is largest over the ITCZ domain (Fig. 8b).

3.2 Application of PGW

We continue with the analysis of the climate change signal obtained from the PGW simulation (see Section 2.2). Figure 9 shows the annual mean spatial distribution of surface precipitation change between CTRL and PGW, and between HIST and SCEN. Marine ITCZ precipitation strongly increases in PGW, in some locations by up to 50% (Fig. 9c). Averaged over the ITCZ and ATL domains, precipitation increases by 7% K^{-1} and 2% K^{-1} respectively. The temperature change for this computation was evaluated at 1 km altitude which roughly corresponds to the cloud base (Fig. 3g). Consistent with the CMIP6-EM (Fig. 9f), the precipitation change in COSMO (Fig. 9c) is most pronounced in the center of the Atlantic, rather than along the West-African coastline (as, e.g., in the MPI-

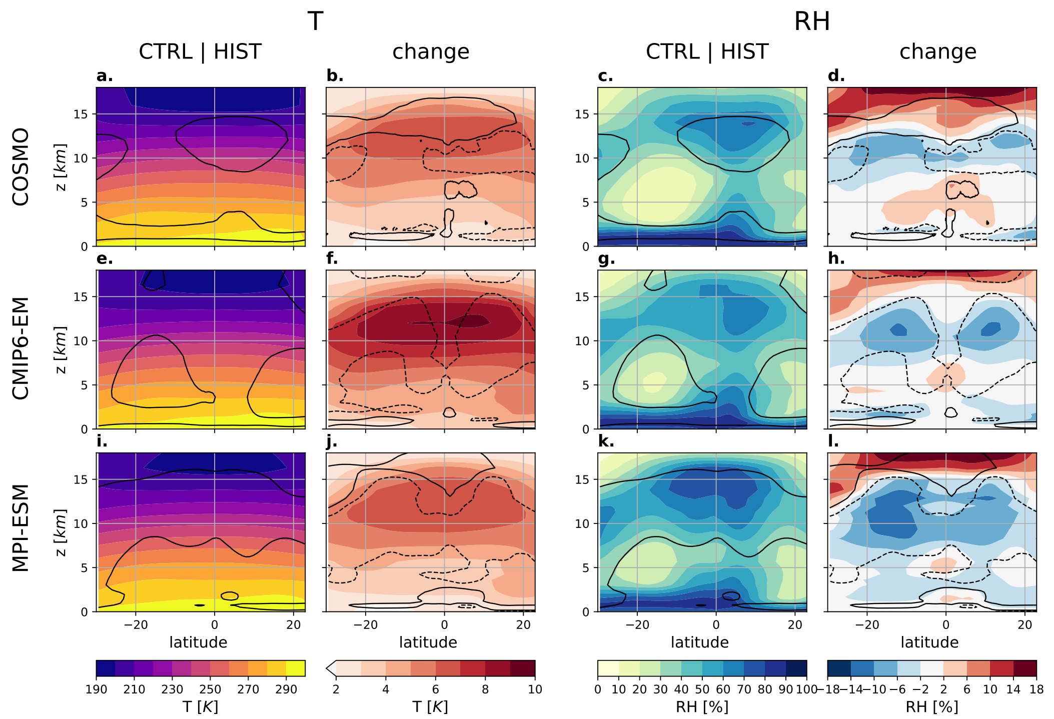

Figure 10. Annual mean altitude-latitude cross-sections of the climate-change signal of (left panels) temperature [K] and (right panels) relative humidity [%] averaged along the longitudes of the HC-CS domain. The panels show (a-d) CTRL and PGW (2007-2010), (e-h) CMIP6-EM HIST (1985-2014) and SCEN (2070-2099), and (i-l) MPI-ESM HIST and SCEN. The first and third columns show CTRL and HIST, while the second and fourth columns show the respective changes PGW−CTRL and SCEN−HIST. Panels (j,l) correspond to the climate delta from the MPI-ESM model used to derive the PGW simulation. The black contour lines indicate (first and third columns) the 5% cloud fraction level and (second and fourth columns) the level of 1% cloud fraction change where solid (dashed) lines represent a positive (negative) change.

ESM; Fig. 9i). Also consistent is the southward propagation of the precipitation maximum, i.e., the most pronounced change is located to the South of the precipitation maximum in CTRL/HIST (see also Fig. 11). However, unlike in the CMIP6-EM, there is no substantial precipitation reduction in the West Atlantic trades, and precipitation over land is reduced, instead of increased. Finally, while the precipitation changes in the CMIP6-EM and the MPI-ESM associated with the ITCZ are relatively symmetric about the equator as a result of the double ITCZ, this is not the case in COSMO which does not show a double ITCZ.

Figure 10 shows the change in the thermodynamic structure of the HC. The temperature change PGW−CTRL (Fig. 10b) is similar to SCEN−HIST of the MPI-ESM (Fig. 10j) but slightly smaller overall. The similarity is expected since the latter is the climate delta used to derive the PGW boundary conditions. Tropospheric relative humidity decreases in the CMIP6 models (Fig. 10h,l) which is a reflection of the overall drying of the tropics, with the exception of a moistening deep-tropical lower troposphere (e.g. Lau & Kim, 2015). COSMO projects a qualitatively similar humidity change pattern (Fig. 10d) as the CMIP6 models, but with a weaker drying of the upper troposphere, a stronger moistening of the lower troposphere in the deep tropics, and – unlike in the CMIP6 models – this signal of increased humidity reaches the subtropics. Note that the relative humidity increase in the tropopause layer in all models appears to be associated with a comparably weak temperature increase due to enhanced longwave radiative cooling (Shine et al., 2003) and enhanced vertical moisture transport (Lau & Kim, 2015).

Figure 11 shows the simulated changes in the cloud field along the HC-CS domain. The signal PGW−CTRL (Fig. 11c) shows a rise of the anvil clouds at the ITCZ accompanied by a strong increase in the high-cloud fraction. In the CMIP6-EM (Fig. 11f), the rise of the high clouds is barely visible in the cloud field change, but will be visible in the meridional wind change (see Fig. 12f). In contrast to COSMO, both the CMIP6-EM (Fig. 11f) and the MPI-ESM (Fig. 11i) exhibit a deep-tropics squeeze, i.e. a reduction of the cloud fraction at the poleward margins of the annual mean ITCZ. Note that this reduction is visible at both instances of the double ITCZ (the real one north of the equator and the spurious one south of the equator). As a result of the deep-tropics squeeze, the ITCZ deep convection and precipitation in SCEN (Fig. 11e,h) is slightly more concentrated around the equator than in HIST (Fig. 11d,g). Finally, we note that the change PGW−CTRL (Fig. 11c) in trade wind clouds exhibits an opposite sign in the North and South Atlantic, unlike in SCEN−HIST (Fig. 11f,i) where shallow cloud cover decreases in both hemispheres.

The circulation changes along the HC-CS domain are shown in Fig. 12 in terms of the meridional and vertical mass fluxes. COSMO simulates an upward shift (maxima rise from approximately 12 km to 14 km) and a shallower upper-level meridional outflow (lower boundary rises more than upper boundary) of the ITCZ in PGW compared to CTRL (Fig. 12a-c). This change pattern qualitatively agrees with the CMIP6-EM (Fig. 12d-f) and the MPI-ESM (Fig. 12g-i), but the change in magnitude is slightly stronger com-

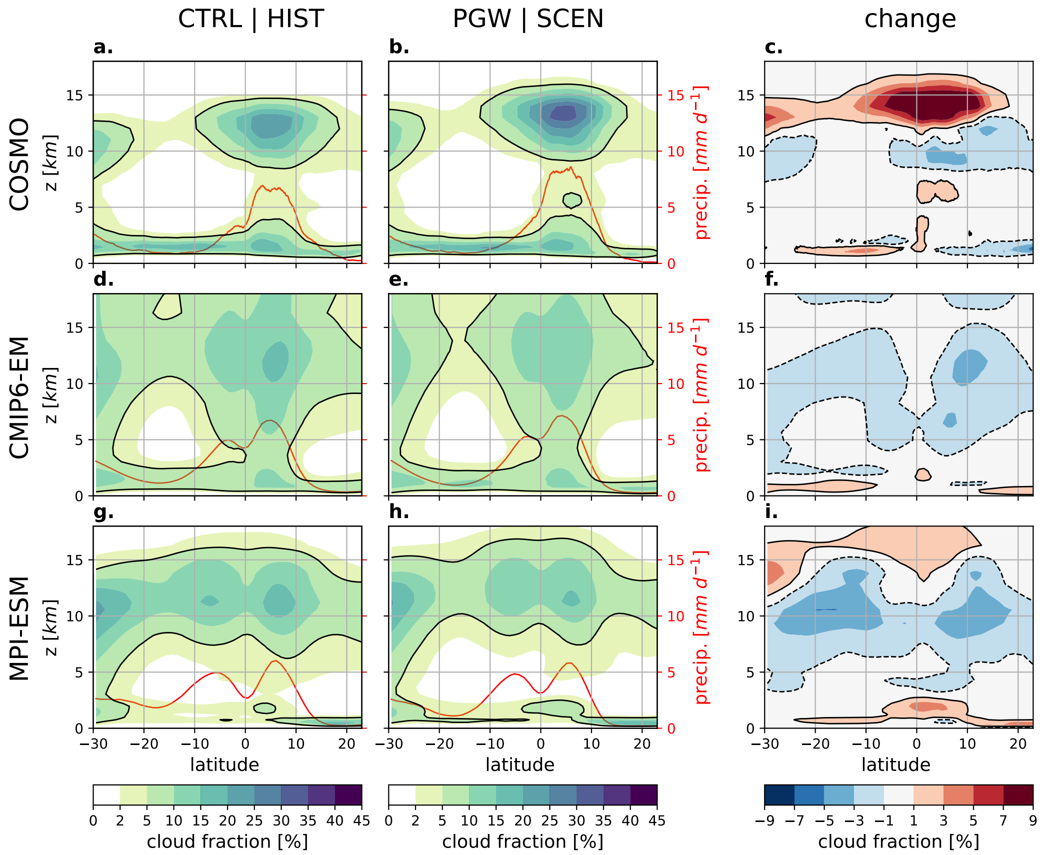

Figure 11. Annual mean altitude-latitude cross-sections of the cloud fraction [%] averaged along the longitudes of the HC-CS domain shown for (a-b) CTRL and PGW (2007-2010), (c) PGW−CTRL, (d) CMIP6-EM HIST (1985-2014), (e) CMIP6-EM SCEN (2070-2099), (f) CMIP6-EM SCEN−HIST, (g) MPI-ESM HIST, (h) MPI-ESM SCEN, and (i) MPI-ESM SCEN−HIST (i.e. corresponding to the climate delta used to derive the PGW simulation). (left and middle panels) The black contour lines high-light the 5% cloud fraction level. The red lines show surface precipitation [mm d^{-1}] represented on the scale of the right y-axis. (right panels) The black contour lines show the 1% level of cloud fraction change where solid (dashed) lines represent a positive (negative) change.

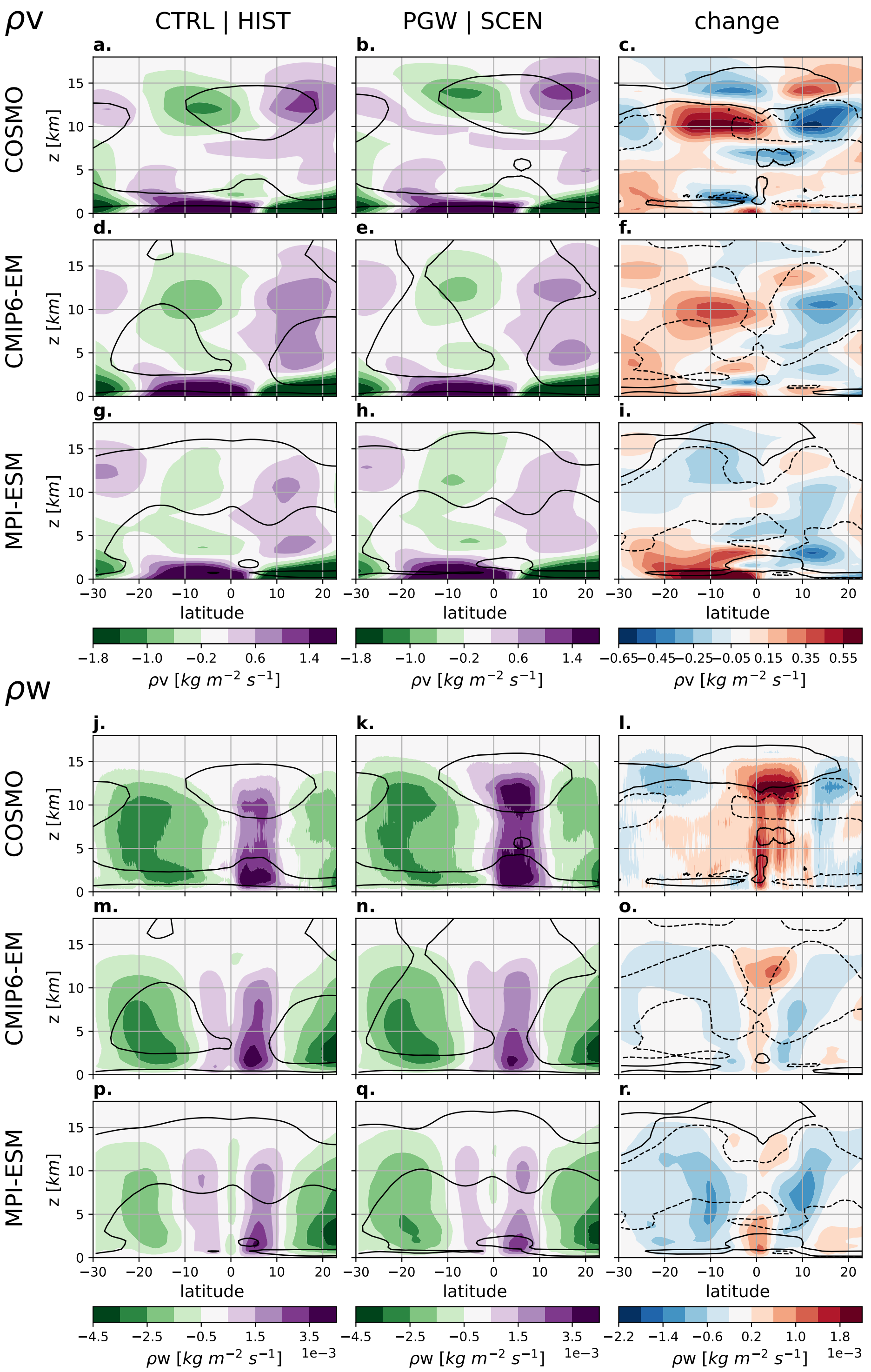

Figure 12. Annual mean altitude-latitude cross-sections of the climate change signal of (a-i) meridional mass flux ρv and (j-r) vertical mass flux ρw [kg m^{-2} s^{-1}] averaged along the longitudes of the HC-CS domain. The panels show (a-c,j-l) CTRL and PGW (2007-2010), (d-f,m-o) CMIP6-EM HIST (1985-2014) and SCEN (2070-2099), and (g-i,p-r) MPI-ESM HIST and SCEN. The first column shows CTRL and HIST, the second PGW and SCEN, and the third column shows the respective changes PGW−CTRL and SCEN−HIST. Panels (i,r) correspond to the climate delta from the MPI-ESM model used to derive the PGW simulation. The black contour lines indicate (first and second columns) the 5% cloud fraction level and (third column) the level of 1% cloud fraction change where solid (dashed) lines represent a positive (negative) change.

pared to the CMIP6-EM, and substantially stronger compared to the MPI-ESM. Along with the change in the meridional wind, the upward motion at the ITCZ in COSMO reaches higher levels and intensifies (Fig. 12j-l). The intensification occurs over the entire tropospheric column, but most pronounced above 10 km altitude. This response of the ITCZ to warming in COSMO shows remarkable differences to the CMIP6 models (Fig. 12m-r): First, the intensification of the ITCZ above 10 km is significantly stronger in COSMO than in the CMIP6 models (compare Figs. 12l and 12o,r), and – with a vertical extension of about 2 km, i.e. from around 13 km to 15 km altitude (Fig. 12j,k) – the deepening of the ITCZ is larger compared to the CMIP6-EM (about 1 km, from around 12 km to 13 km, Fig. 12m,n). Second, the change of the ITCZ below 10 km represents a response that differs from the deep-tropics squeeze. While the CMIP6 models simulate a weakening of the upward motion at the margins of the deep-tropics and only a weak intensification at the equator (i.e. the deep-tropics squeeze; Fig. 12o,r), COSMO simulates an extension of the ITCZ towards south and an intensification over the entire meridional extent of the CTRL ITCZ (Fig. 12j,l).

With respect to subtropical subsidence, the response of COSMO also differs from the CMIP6 models. First, the strengthening of subsidence is mostly confined to the edge of the cloud anvils above 10 km and extends less prominently through the tropospheric column than in the CMIP6-EM and the MPI-ESM. In the northern hemisphere, the subsidence intensification below 10 km is still comparable to the CMIP6 models (even though confined to the subtropics), but in the southern hemisphere, there is an overall weakening of annual mean subsidence in COSMO, as opposed to the strengthening in the CMIP6 models. Finally, the intensification of subtropical subsidence above 10 km is substantially larger in COSMO than in the CMIP6-EM, consistent with the more pronounced deepening and upper-level intensification of the ITCZ deep convection.

4 Discussion

4.1 Evaluation of CTRL

In Section 3, we discussed the realism of the ERA5-driven CTRL simulation in comparison to the CMIP6-EM and found significant differences. As the two underlying simulation strategies differ strongly, it is not feasible to disentangle effects due to computational resolution (3 km versus 50-200 km) and simulation setup (ERA5 driven atmospheric simulations versus free-running coupled simulations). The main purpose of the following discussion is thus to summarize the differences between the CTRL simulation and the CMIP6 ensemble, and to determine whether the ERA5-driven simulations are credible enough to serve as the basis of climate-change simulations using the PGW approach.

The improved representation of the annual cycle of the albedo, in particular on the TRD analysis domain (representative of shallow cumulus clouds), as well as the accurate vertical structure and meridional position of the ITCZ (i.e. no double ITCZ) are perhaps the most promising improvements compared to the CMIP6-EM. The prescribed SST obtained from ERA5 likely has a beneficial impact on the properties of the MBL and the position of the ITCZ in CTRL. For instance, the double ITCZ problem of the CMIP6-EM is thought to be related to air-sea interaction, among other factors (Lin, 2007; Li & Xie, 2014). It would therefore be interesting to test if for instance a coupled model setup at kilometer-resolution or a GCM-driven kilometer-resolution simulation were to suffer from the double ITCZ problem. Under the assumption that the improved representation of the ITCZ in our limited-area CTRL simulation is due to the forcing from ERA5, our application demonstrates one benefit of the PGW approach compared to conventional downscaling, i.e. that GCM circulation biases are not propagated to the limited-area simulation. We argue that this realistic representation of the ITCZ location is a good starting point to study its climate change signal.

Concerning the simulation of low clouds, the representation of the annual cycle of the albedo in CTRL is better on the TRD domain than on the STC domain. This discrepancy may relate to the type of clouds most prevalent on the two domains. The TRD domain is predominantly covered by trade-wind cumulus clouds while stratocumulus clouds are more frequent on the STC domain (Warren et al., 1988). The difficulty to represent the annual cycle of stratocumulus clouds in a kilometer-resolution model with 60 vertical levels is not unexpected since a firm representation of the stratocumulus-topped MBL with its very shallow inversion cloud layer is challenging even in LES (e.g. Stevens et al., 2005). Nevertheless, the fact that the COSMO simulations yield stratocumulus decks already at kilometer-resolution, notably without any shallow convection scheme, is very promising. In the trade-wind cumulus regime clouds often aggregate into clusters that frequently exceed the kilometer-scale (e.g. Bony et al., 2020). The CTRL simulation indeed produces such clusters (see Fig. 2) suggesting that some of the dominant mesoscale patterns of MBL circulations and clouds in the Trades are at least partially resolved. Similar results have been found in previous studies using kilometer-resolution models (Klocke et al., 2017; Heim et al., 2021; Caldwell et al., 2021). It is interesting to note that the annual cycle of albedo in CTRL on the TRD domain is actually better simulated than in ERA5. This result suggests that the improved representation of these clouds is not primarily a result of the prescribed SST, but portrays the added value of explicit convection and fine model resolution.

On the other hand, we find a mean bias in the low-cloud albedo in the CTRL simulation compared to satellite observations (Fig. 5). This bias was found to be caused by an overestimation of cloud water (i.e., cloud opacity) rather than cloud fraction (Heim et al., 2021). As shown by Liu et al. (2022), this bias of the COSMO model at kilometer-resolution can be reduced through systematic model calibration. The model version used here is still based on a set of empirical parameters that were calibrated for applications over continental regions of the mid-latitudes (Bellprat et al., 2016). We also find a bias in quantities related to deep convection at the continental ITCZ over Africa (Fig. 5). Compared to the well calibrated COSMO simulations in the mid-latitudes (e.g. Leutwyler et al., 2017; Vergara-Temprado et al., 2020; Ban et al., 2021; Zeman et al., 2021), the bias in precipitation and OLR is still quite substantial. The set of empirical parameters used in this study differs from other COSMO setups that have been used over Africa (Bucchignani et al., 2016; Sørland et al., 2021). A calibration effort similar as it was done for the tropical Atlantic in Liu et al. (2022), but for continental Africa would likely result in a simulation setup with less biased deep convection overall. Note, it is possible that the poor representation of the continental ITCZ could affect the representation of the marine ITCZ via the lower-tropospheric mean easterly flow or via gravity waves (e.g. Leutwyler & Hohenegger, 2021).

4.2 Climate Change Signal PGW−CTRL

The changes SCEN−HIST in wind and humidity at the Atlantic HC compare qualitatively well to the the global CMIP5 models (Lau & Kim, 2015). This agreement indicates that, despite the local computational domain employed, the obtained results may be indicative of the global patterns. Concerning the change signal in COSMO (PGW−CTRL), the tropospheric warming profile closely follows the climate delta (SCEN−HIST) of the MPI-ESM simulation (Fig. 10). This similarity is expected since the temperature change is a large-scale signal that enters the model at the lateral boundaries (see Sec. 2.2). The change signal PGW−CTRL for humidity shows a qualitatively similar change pattern as the CMIP6-EM and the MPI-ESM, however, with an overall weaker drying of the tropical atmosphere (Fig. 10). The distribution of humidity is tied to the representation of deep convection and how it changes between CTRL and PGW (or HIST and SCEN). Since domain-average convection at the ITCZ intensifies in COSMO but weakens in the MPI-ESM model, some differences in the humidity change are expected.

The circulation changes, on the other hand, differ quite substantially between COSMO and the CMIP6 models. The intensification of deep convection at the ITCZ is remarkably strong and accompanied by a widening of the ITCZ in the presented kilometer-resolution simulation. This result is novel, since GCM projections show an anti-correlation between strengthening and widening of the ITCZ between models (Byrne et al., 2018). Also, the rise of the anvil clouds is more pronounced than in the CMIP6 models, and the increase in the anvil cloud fraction is even contrary to the expectation of the stability iris hypothesis (Bony et al., 2016). In this respect, our simulation qualitatively differs from high-resolution simulations of radiative-convective equilibrium in aqua-planet configurations, whereof a majority shows a reduction in the high-cloud fraction with warming (Wing et al., 2020). Yet, the increase in tropical high clouds shows similarities to the response Satoh et al. (2012) found in their global kilometer-resolution short-term climate simulation. For this simulation, Tsushima et al. (2014) determined that the change in high ice clouds is sensitive to the formulation of subgrid turbulent mixing. The work of Tsushima et al. (2014); Ohno and Satoh (2018); Ohno et al. (2019, 2021) demonstrates that even at kilometer-resolution the response of tropical deep convection to warming may be subject to extensive inter-model variability, and that the here presented results require corroboration from kilometer-resolution climate simulations employing other model codes, microphysics schemes, and downscaling approaches.

An often discussed hypothesis on the change in the dynamics of the HC is the prominent deep-tropics squeeze, i.e. the narrowing of the annual mean ITCZ, detectable in GCMs (e.g. Lau & Kim, 2015; Byrne & Schneider, 2016). In our CMIP6 ensemble, the squeeze is clearly evident in the form of a strengthening and narrowing of the deep-tropical convection and a corresponding reduction of cloud fraction at the edges of the ITCZ (Fig. 11 and Fig. 12). However, this narrowing of the annual mean ITCZ seems to be enhanced by the fact that the CMIP6-EM projects a similar but mirrored change signal at both branches of the ITCZ (i.e. the one north of the equator, and the spurious one south of the equator – the double ITCZ). This perception is supported by the fact that the narrowing of the ITCZ in GCMs is associated mainly with a northward shift of the southern edge (Byrne & Schneider, 2016). The deep-tropics squeeze can not be visually detected in the kilometer-resolution simulation which does not produce a double ITCZ in CTRL. So, the question arises whether the narrowing of the deep tropics in the CMIP6-EM would be equally pronounced if it did not exhibit the double ITCZ in HIST. The circulation changes projected by COSMO differ more prominently from CMIP6-EM at the southern edge of the ITCZ, suggesting that the double ITCZ may indeed contribute to the differences in the projected change. The double ITCZ was found to relate to the strength of the low-cloud feedback in GCMs (Tian, 2015) which was argued to be driven by differences in the lower-tropospheric stability depending on the strength of the double ITCZ (Webb & Lock, 2020). Whether and how the double ITCZ responds to warming and how this relates to radiative feedbacks is thus of high relevance for climate projections and requires further research.

There are some limitations of the model setup presented in this study. The COSMO model was originally designed as a weather prediction model, and aerosols and ozone are represented in a simplified manner compared to comprehensive climate models. Further, the one-moment microphysics scheme assumes a constant cloud-droplet number concentration. Changes in aerosol concentrations therefore do not directly alter the properties of the simulated clouds. Keeping ozone and aerosol concentrations constant between CTRL and PGW is thus a pragmatic choice for the given model configuration. Still, accounting for such effects might alter the simulated response to warming. For instance, the MPI-ESM shows an increase and slight upward shift of the ozone maximum between HIST and SCEN. Another simplification of the modelling setup in this study is the use of a limited-area model and the PGW approach. Given that the same weather enters the model domain at the boundaries in CTRL and PGW, large-scale circulation changes from the GCM may be restrained by the persistence of the weather phenomena at the lateral boundaries. Specifically, at the boundary between the subtropics and the mid-latitudes, it is unclear how the extension of the HC towards South with warming (e.g. Lau & Kim, 2015) is restrained by the fact that the mid-latitude frontal systems enter the PGW simulation at the same latitudes as in CTRL.

An interesting extension of this study would be to repeat the analysis using PGW simulations derived with climate deltas of different GCMs to test the sensitivity of the change signal PGW−CTRL to the climate delta. The role of SST warming patterns appears to be of particular interest here. Given the importance of the SST pattern on changes of the ITCZ (Huang et al., 2013), it would not be surprising to find differences in the change PGW−CTRL in terms of structure and location of the ITCZ for different climate deltas.

5 Conclusion

In this study, we conducted what is, to our best knowledge, the first application of the pseudo-global warming (PGW) approach on a marine tropical domain that contains the entire Hadley circulation. We performed two 4-year-long simulations at 3.3 km horizontal resolution with the limited-area model COSMO over the tropical Atlantic. The analysis includes an evaluation of the structure of the Hadley circulation and tropical clouds under current climate conditions (CTRL), and a comparison of the obtained climate change signal (PGW−CTRL) to that of a CMIP6 model ensemble (SCEN−HIST). The radiative feedback between CTRL and PGW will be analysed in a follow-up study. The main analysis findings include:

1. An improved representation of the vertical structure and seasonal cycle (in terms of the meridional location) of the Atlantic ITCZ compared to the CMIP6 ensemble. In particular, our limited area simulation with explicit convection does not suffer from the double ITCZ problem.
2. An improved representation of the annual cycle of the TOA albedo compared to the CMIP6 ensemble, in particular in the trade-wind cumulus region where CTRL even outperforms the ERA5 reanalysis. This suggests that kilometer-resolution simulations are a suitable tool to study cloud feedbacks in the trade-wind region. Despite disabling the models shallow convection scheme, stratocumulus clouds are evident, albeit somewhat too frequent, and with an underestimated amplitude of the annual cycle.
3. The dynamics of the ITCZ respond to warming in a different way in our kilometer-resolution simulation compared to the analysed GCMs. While the CMIP6 ensemble shows a narrowing and central intensification of the ITCZ, i.e. a prominent

deep-tropics squeeze, the kilometer-resolution simulation shows an overall intensification of the ITCZ, most pronounced at high altitudes, and a slight extension towards south.

Overall, our results demonstrate the merit of high-resolution climate simulations in a real-world configuration to compare against GCM projections. kilometer-resolution models enable an unprecedented view on tropical clouds and circulations from the large-scale tropical overturning circulation down to small-scale convective MBL circulations and clouds. Even though global kilometer-resolution climate simulations are not yet feasible, our study demonstrates that downscaling strategies like the PGW approach allow to gain insights from these models already today. We presented one such simulation that, compared to GCMs, produces a remarkably different climate-change response for the HC and in particular for the ITCZ. The realism of this response is difficult to assess as long as such simulations remain a rarity. We will analyse in more detail the cause of the response in upcoming work.

6 Data Availability

The CERES EBAF TOA radiation data are available at `https://ceres-tool.larc.nasa.gov/ord-tool/jsp/EBAFTOA41Selection.jsp` via `DOI:10.5067/TERRA-AQUA/CERES/EBAF-TOA_L3B004.1`.
The CM SAF TOA radiation data are available at `https://wui.cmsaf.eu/safira/action/viewProduktList?dId=3` via `DOI:10.5676/EUM_SAF_CM/TOA_GERB/V002`.
The GPM IMERG precipitation data are available at `https://disc.gsfc.nasa.gov` via `DOI:10.5067/GPM/IMERGDF/DAY/06`.
The ERA5 reanalysis data are available at the Copernicus Climate Change Service (C3S) Climate Data Store via `DOI:10.24381/cds.bd0915c6`.
The CMIP6 data are available at the `https://esgf-node.llnl.gov/projects/cmip6/`.
The software to prepare PGW simulations can be obtained from `https://github.com/Potopoles/pgw-python` via `DOI:10.5281/zenodo.6759029`.
The weather and climate model COSMO is free of charge for research applications (for more details see: `http://www.cosmo-model.org`).

Acknowledgments

This work was funded by the Swiss National Science Foundation (SNSF) project "Exploiting km-resolution climate models in the tropics to constrain climate change uncertainties" (trCLIM).

We acknowledge PRACE for awarding us access to Piz Daint at Swiss National Supercomputing Center (CSCS, Switzerland). Furthermore, we acknowledge the COSMO, CLM and C2SM communities for developing and maintaining COSMO in climate mode, and the Federal Office for Meteorology and Climatology MeteoSwiss, CSCS, and ETH Zürich for their contributions to the development of the GPU-accelerated version of COSMO.

We acknowledge the World Climate Research Programme, which, through its Working Group on Coupled Modelling, coordinated and promoted CMIP6. We thank the climate modeling groups for producing and making available their model output, the Earth System Grid Federation (ESGF) for archiving the data and providing access, and the multiple funding agencies who support CMIP6 and ESGF.

References

Adachi, S. A., & Tomita, H. (2020). Methodology of the Constraint Condition in Dynamical Downscaling for Regional Climate Evaluation: A Review. *Journal of Geophysical Research: Atmospheres*, *125*(11). doi: 10.1029/2019JD032166

Baldauf, M., Seifert, A., Förstner, J., Majewski, D., Raschendorfer, M., & Reinhardt, T. (2011, 12). Operational Convective-Scale Numerical Weather Prediction with the COSMO Model: Description and Sensitivities. *Monthly Weather Review*, *139*(12), 3887–3905. Retrieved from `http://journals.ametsoc.org/doi/abs/10.1175/MWR-D-10-05013.1` doi: 10.1175/MWR-D-10-05013.1

Ban, N., Caillaud, C., Coppola, E., Pichelli, E., Sobolowski, S., Adinolfi, M., ... Zander, M. J. (2021, 7). The first multi-model ensemble of regional climate simulations at kilometer-scale resolution, part I: evaluation of precipitation. *Climate Dynamics*, *57*(1-2), 275–302. Retrieved from `https://doi.org/10.1007/s00382-021-05708-whttps://link.springer.com/10.1007/s00382-021-05708-w` doi: 10.1007/s00382-021-05708-w

Bellprat, O., Kotlarski, S., Lüthi, D., De Elía, R., Frigon, A., Laprise, R., & Schär, C. (2016). Objective calibration of regional climate models: Application over Europe and North America. *Journal of Climate*, *29*(2), 819–838. doi:

10.1175/JCLI-D-15-0302.1

Bellucci, A., Gualdi, S., & Navarra, A. (2010, 3). The double-ITCZ syndrome in coupled general circulation models: The role of large-scale vertical circulation regimes. *Journal of Climate*, *23*(5), 1127–1145. doi: 10.1175/2009JCLI3002.1

Belušić, A., Prtenjak, M. T., Güttler, I., Ban, N., Leutwyler, D., & Schär, C. (2018, 6). Near-surface wind variability over the broader Adriatic region: insights from an ensemble of regional climate models. *Climate Dynamics*, *50*(11-12), 4455–4480. Retrieved from http://dx.doi.org/10.1007/s00382-017-3885-5http://link.springer.com/10.1007/s00382-017-3885-5 doi: 10.1007/s00382-017-3885-5

Blossey, P. N., Bretherton, C. S., Zhang, M., Cheng, A., Endo, S., Heus, T., … Xu, K. (2013, 6). Marine low cloud sensitivity to an idealized climate change: The CGILS LES intercomparison. *Journal of Advances in Modeling Earth Systems*, *5*(2), 234–258. Retrieved from https://onlinelibrary.wiley.com/doi/10.1002/jame.20025 doi: 10.1002/jame.20025

Bony, S., & Dufresne, J.-L. (2005). Marine boundary layer clouds at the heart of tropical cloud feedback uncertainties in climate models. *Geophysical Research Letters*, *32*(20), L20806. Retrieved from http://doi.wiley.com/10.1029/2005GL023851 doi: 10.1029/2005GL023851

Bony, S., Schulz, H., Vial, J., & Stevens, B. (2020, 4). Sugar, Gravel, Fish, and Flowers: Dependence of Mesoscale Patterns of Trade-Wind Clouds on Environmental Conditions. *Geophysical Research Letters*, *47*(7). doi: 10.1029/2019GL085988

Bony, S., Stevens, B., Coppin, D., Becker, T., Reed, K. A., Voigt, A., & Medeiros, B. (2016). Thermodynamic control of anvil cloud amount. *Proceedings of the National Academy of Sciences of the United States of America*, *113*(32), 8927–8932. doi: 10.1073/pnas.1601472113

Bott, A. (1989, 5). A Positive Definite Advection Scheme Obtained by Nonlinear Renormalization of the Advective Fluxes. *Monthly Weather Review*, *117*(5), 1006–1016. Retrieved from https://doi.org/10.1175/1520-0493(1989)117%3C1006:APDASO%3E2.0.COhttp://0.0.0.2 doi: 10.1175/1520-0493(1989)117⟨1006:APDASO⟩2.0.CO;2

Bretherton, C. S. (2015, 11). Insights into low-latitude cloud feedbacks from high-resolution models. *Philosophical Transactions of the Royal Society A: Mathematical, Physical and Engineering Sciences*, *373*(2054), 20140415. Retrieved from https://royalsocietypublishing.org/doi/10.1098/rsta.2014.0415 doi: 10.1098/rsta.2014.0415

Bretherton, C. S., & Wyant, M. C. (1997, 1). Moisture Transport, Lower-Tropospheric Stability, and Decoupling of Cloud-Topped Boundary Layers. *Journal of the Atmospheric Sciences*, *54*(1), 148–167. Retrieved from https://doi.org/10.1175/1520-0469(1997)054%3C0168:NSAACM%3E2.0.CO;2http://journals.ametsoc.org/doi/abs/10.1175/1520-0469%281997%29054%3C0148%3AMTLTSA%3E2.0.CO%3B2 doi: 10.1175/1520-0469(1997)054⟨0148:MTLTSA⟩2.0.CO;2

Brogli, R., Heim, C., Sørland, S. L., & Schär, C. (2022). The pseudo-global-warming (PGW) approach: Methodology, software package PGW4ERA5 v1.1, validation and sensitivity analyses. *Geoscientific Model Development*, *in review*. doi: 10.5194/gmd-2022-167

Brogli, R., Kröner, N., Sørland, S. L., Lüthi, D., & Schär, C. (2019, 1). The Role of Hadley Circulation and Lapse-Rate Changes for the Future European Summer Climate. *Journal of Climate*, *32*(2), 385–404. Retrieved from http://journals.ametsoc.org/doi/10.1175/JCLI-D-18-0431.1 doi: 10.1175/JCLI-D-18-0431.1

Bucchignani, E., Cattaneo, L., Panitz, H. J., & Mercogliano, P. (2016, 2). Sensitivity analysis with the regional climate model COSMO-CLM over the CORDEX-MENA domain. *Meteorology and Atmospheric Physics*, *128*(1), 73–95. doi: 10.1007/s00703-015-0403-3

Byrne, M. P., Pendergrass, A. G., Rapp, A. D., & Wodzicki, K. R. (2018, 12). *Response of the Intertropical Convergence Zone to Climate Change: Location, Width, and Strength* (Vol. 4) (No. 4). Springer. doi: 10.1007/s40641-018-0110-5

Byrne, M. P., & Schneider, T. (2016, 11). Narrowing of the ITCZ in a warming climate: Physical mechanisms. *Geophysical Research Letters*, *43*(21), 350–11. Retrieved from https://onlinelibrary.wiley.com/doi/10.1002/2016GL070396 doi: 10.1002/2016GL070396

Caldwell, P. M., Terai, C. R., Hillman, B., Keen, N. D., Bogenschutz, P., Lin, W.,

... Zender, C. S. (2021, 11). Convection-Permitting Simulations With the E3SM Global Atmosphere Model. *Journal of Advances in Modeling Earth Systems*, *13*(11). doi: 10.1029/2021MS002544

Chen, J., Wang, Z., Tam, C.-Y., Lau, N.-C., Lau, D.-S. D., & Mok, H.-Y. (2020, 12). Impacts of climate change on tropical cyclones and induced storm surges in the Pearl River Delta region using pseudo-global-warming method. *Scientific Reports*, *10*(1), 1965. doi: 10.1038/s41598-020-58824-8

Clerbaux, N., Nevens, S., & Decoster, I. (2013). CM SAF TOA Radiation "GERB" dataset - Edition 1 - Monthly Means / Daily Means / Monthly mean diurnal cycle, Satellite Application Facility on Climate Monitoring.

Copernicus Climate Change Service (C3S). (2017). ERA5: Fifth generation of ECMWF atmospheric reanalyses of the global climate. *Copernicus Climate Change Service Climate Data Store (CDS)*. Retrieved from `https://cds.climate.copernicus.eu/cdsapp#!/home`

Eyring, V., Bony, S., Meehl, G. A., Senior, C. A., Stevens, B., Stouffer, R. J., & Taylor, K. E. (2016, 5). Overview of the Coupled Model Intercomparison Project Phase 6 (CMIP6) experimental design and organization. *Geoscientific Model Development*, *9*(5), 1937–1958. Retrieved from `https://gmd.copernicus.org/articles/9/1937/2016/` doi: 10.5194/gmd-9-1937-2016

Fiedler, S., Crueger, T., D'Agostino, R., Peters, K., Becker, T., Leutwyler, D., ... Stevens, B. (2020, 9). Simulated Tropical Precipitation Assessed across Three Major Phases of the Coupled Model Intercomparison Project (CMIP). *Monthly Weather Review*, *148*(9), 3653–3680. Retrieved from `http://journals.ametsoc.org/doi/10.1175/MWR-D-19-0404.1` doi: 10.1175/MWR-D-19-0404.1

Forster, P., Storelvmo, T., Armour, K., Collins, W., Dufresne, J.-l., Frame, D., ... Zhang, H. (2021). *The Earth's Energy Budget, Climate Feedbacks, and Climate Sensitivity. In Climate Change 2021: The Physical Science Basis. Contribution of Working Group I to the Sixth Assessment Report of the Intergovernmental Panel on Climate Change [Masson-Delmotte, V., P. Zhai, A. Pirani, S.L. Connors, C. Péan, S. Berger, N. Caud, Y. Chen, L. Goldfarb, M.I. Gomis, M. Huang, K. Leitzell, E. Lonnoy, J.B.R. Matthews, T.K.*

Maycock, T. Waterfield, O. Yelekçi, R. Yu, and B. Zhou (eds.)]. Cambridge, United Kingdom and New York, NY, USA: Cambridge University Press. doi: 10.1017/9781009157896.009

Fuhrer, O., Osuna, C., Lapillonne, X., Gysi, T., Cumming, B., Bianco, M., . . . Schulthess, T. C. (2014, 9). Towards a performance portable, architecture agnostic implementation strategy for weather and climate models. *Supercomputing Frontiers and Innovations*, *1*(1), 44–61. Retrieved from `http://superfri.org/superfri/article/view/17` doi: 10.14529/jsfi140103

Hartmann, D. L., & Larson, K. (2002, 10). An important constraint on tropical cloud - climate feedback. *Geophysical Research Letters*, *29*(20), 12–1. Retrieved from `http://doi.wiley.com/10.1029/2002GL015835` doi: 10.1029/2002GL015835

Heim, C., Hentgen, L., Ban, N., & Schär, C. (2021). Inter-model Variability in Convection-Resolving Simulations of Subtropical Marine Low Clouds. *Journal of the Meteorological Society of Japan. Ser. II*, *99*(5), 2021–062. Retrieved from `https://www.jstage.jst.go.jp/article/jmsj/99/5/99_2021-062/_article` doi: 10.2151/jmsj.2021-062

Heise, E., Lange, M., Ritter, B., & Schrodin, R. (2003). Improvement and validation of the multilayer soil model. *COSMO Newsletter*, *3*, 198–203. Retrieved from `http://www.cosmo-model.org`

Held, I. M., & Hou, A. Y. (1980, 3). Nonlinear Axially Symmetric Circulations in a Nearly Inviscid Atmosphere. *Journal of the Atmospheric Sciences*, *37*(3), 515–533. Retrieved from `http://journals.ametsoc.org/doi/10.1175/1520-0469(1980)037<0515:NASCIA>2.0.CO;2` doi: 10.1175/1520-0469(1980)037⟨0515:NASCIA⟩2.0.CO;2

Hentgen, L., Ban, N., Kröner, N., Leutwyler, D., & Schär, C. (2019, 4). Clouds in Convection-Resolving Climate Simulations Over Europe. *Journal of Geophysical Research: Atmospheres*, *124*(7), 3849–3870. Retrieved from `https://onlinelibrary.wiley.com/doi/abs/10.1029/2018JD030150` doi: 10.1029/2018JD030150

Hersbach, H., Bell, B., Berrisford, P., Hirahara, S., Horányi, A., Muñoz-Sabater, J., . . . Thépaut, J. (2020, 7). The ERA5 global reanalysis. *Quarterly Journal of the Royal Meteorological Society*, *146*(730), 1999–2049. Retrieved from https://onlinelibrary.wiley.com/doi/abs/10.1002/qj.3803https://onlinelibrary.wiley.com/doi/10.1002/qj.3803 doi: 10.1002/qj.3803

Hohenegger, C., Kornblueh, L., Klocke, D., Becker, T., Cioni, G., Engels, J. F., ... Stevens, B. (2020). Climate Statistics in Global Simulations of the Atmosphere, from 80 to 2.5 km Grid Spacing. *Journal of the Meteorological Society of Japan. Ser. II*, *98*(1), 73–91. Retrieved from https://www.jstage.jst.go.jp/article/jmsj/98/1/98_2020-005/_article doi: 10.2151/jmsj.2020-005

Huang, P., Xie, S.-P., Hu, K., Huang, G., & Huang, R. (2013, 5). Patterns of the seasonal response of tropical rainfall to global warming. *Nature Geoscience*, *6*(5), 357–361. Retrieved from http://www.nature.com/articles/ngeo1792 doi: 10.1038/ngeo1792

Huffman, G., E.F. Stocker, D.T. Bolvin, E.J. Nelkin, & Jackson Tan. (2019). *GPM IMERG Final Precipitation L3 1 day 0.1 degree x 0.1 degree V06, Edited by Andrey Savtchenko, Greenbelt, MD, Goddard Earth Sciences Data and Information Services Center (GES DISC), Accessed: 06.07.2022.* doi: 10.5067/GPM/IMERGDF/DAY/06

Jenney, A. M., Randall, D. A., & Branson, M. D. (2020, 6). Understanding the Response of Tropical Ascent to Warming Using an Energy Balance Framework. *Journal of Advances in Modeling Earth Systems*, *12*(6). doi: 10.1029/2020MS002056

Kawai, H., & Shige, S. (2020). Marine Low Clouds and their Parameterization in Climate Models. *Journal of the Meteorological Society of Japan. Ser. II*, *98*(6), 1097–1127. Retrieved from https://www.jstage.jst.go.jp/article/jmsj/98/6/98_2020-059/_article doi: 10.2151/jmsj.2020-059

Klemp, J. B., & Durran, D. R. (1983, 3). An Upper Boundary Condition Permitting Internal Gravity Wave Radiation in Numerical Mesoscale Models. *Monthly Weather Review*, *111*(3), 430–444. Retrieved from http://journals.ametsoc.org/doi/10.1175/1520-0493(1983)111%3C0430:AUBCPI%3E2.0.CO;2 doi: 10.1175/1520-0493(1983)111⟨0430:AUBCPI⟩2.0.CO;2

Klemp, J. B., & Wilhelmson, R. B. (1978, 6). The Simulation of Three-Dimensional Convective Storm Dynamics. *Journal of the Atmospheric Sciences*, *35*(6), 1070–1096. Retrieved from http://journals.ametsoc.org/

doi/10.1175/1520-0469(1978)035<1070:TSOTDC>2.0.CO;2 doi: 10.1175/1520-0469(1978)035⟨1070:TSOTDC⟩2.0.CO;2

Klocke, D., Brueck, M., Hohenegger, C., & Stevens, B. (2017, 12). Rediscovery of the doldrums in storm-resolving simulations over the tropical Atlantic. *Nature Geoscience*, *10*(12), 891–896. Retrieved from http://dx.doi.org/10.1038/s41561-017-0005-4http://www.nature.com/articles/s41561-017-0005-4 doi: 10.1038/s41561-017-0005-4

Kriegler, E., Bauer, N., Popp, A., Humpenöder, F., Leimbach, M., Strefler, J., ... Edenhofer, O. (2017, 1). Fossil-fueled development (SSP5): An energy and resource intensive scenario for the 21st century. *Global Environmental Change*, *42*, 297–315. Retrieved from https://linkinghub.elsevier.com/retrieve/pii/S0959378016300711 doi: 10.1016/j.gloenvcha.2016.05.015

Kröner, N., Kotlarski, S., Fischer, E., Lüthi, D., Zubler, E., & Schär, C. (2017, 5). Separating climate change signals into thermodynamic, lapse-rate and circulation effects: theory and application to the European summer climate. *Climate Dynamics*, *48*(9-10), 3425–3440. Retrieved from http://link.springer.com/10.1007/s00382-016-3276-3 doi: 10.1007/s00382-016-3276-3

Lau, W. K. M., & Kim, K.-M. (2015, 3). Robust Hadley Circulation changes and increasing global dryness due to CO 2 warming from CMIP5 model projections. *Proceedings of the National Academy of Sciences*, *112*(12), 3630–3635. Retrieved from https://pnas.org/doi/full/10.1073/pnas.1418682112 doi: 10.1073/pnas.1418682112

Lau, W. K. M., Kim, K. M., Chern, J. D., Tao, W. K., & Leung, L. R. (2020, 1). Structural changes and variability of the ITCZ induced by radiation–cloud–convection–circulation interactions: inferences from the Goddard Multi-scale Modeling Framework (GMMF) experiments. *Climate Dynamics*, *54*(1-2), 211–229. doi: 10.1007/s00382-019-05000-y

Leutwyler, D., Fuhrer, O., Lapillonne, X., Lüthi, D., & Schär, C. (2016). Towards European-scale convection-resolving climate simulations with GPUs: A study with COSMO 4.19. *Geoscientific Model Development*, *9*(9), 3393–3412. doi: 10.5194/gmd-9-3393-2016

Leutwyler, D., & Hohenegger, C. (2021). Weak cooling of the troposphere by tropical islands in simulations of the radiative-convective equilibrium. *Quar-*

terly Journal of the Royal Meteorological Society, *147*(736), 1788–1800. doi: 10.1002/qj.3995

Leutwyler, D., Lüthi, D., Ban, N., Fuhrer, O., & Schär, C. (2017, 5). Evaluation of the convection-resolving climate modeling approach on continental scales. *Journal of Geophysical Research: Atmospheres*, *122*(10), 5237–5258. Retrieved from `http://doi.wiley.com/10.1002/2016JD026013` doi: 10.1002/2016JD026013

Li, G., & Xie, S. P. (2014). Tropical biases in CMIP5 multimodel ensemble: The excessive equatorial pacific cold tongue and double ITCZ problems. *Journal of Climate*, *27*(4), 1765–1780. doi: 10.1175/JCLI-D-13-00337.1

Lin, J. L. (2007, 9). The double-ITCZ problem in IPCC AR4 coupled GCMs: Ocean-atmosphere feedback analysis. *Journal of Climate*, *20*(18), 4497–4525. doi: 10.1175/JCLI4272.1

Liu, S., Zeman, C., Sørland, S. L., & Schär, C. (2022). Systematic Calibration of A Convection-Resolving Model: Application over Tropical Atlantic. *submitted to Journal of Geophysical Research: Atmospheres*.

Loeb, N. G., Doelling, D. R., Wang, H., Su, W., Nguyen, C., Corbett, J. G., … Kato, S. (2018, 1). Clouds and the Earth's Radiant Energy System (CERES) Energy Balanced and Filled (EBAF) Top-of-Atmosphere (TOA) Edition-4.0 Data Product. *Journal of Climate*, *31*(2), 895–918. Retrieved from `http://journals.ametsoc.org/doi/10.1175/JCLI-D-17-0208.1` doi: 10.1175/JCLI-D-17-0208.1

Mechoso, C., Robertson, A., Barth, N., Davey, M., Delecluse, P., Gent, P., … Tribbia, J. (1995, 9). The Seasonal Cycle over the Tropical Pacific in Coupled Ocean–Atmosphere General Circulation Models. *Monthly Weather Review*, *123*(9), 2825–2838. doi: 10.1175/1520-0493(1995)123⟨2825:TSCOTT⟩2.0.CO;2

Nakamura, R., & Mäll, M. (2021, 12). Pseudo Global Warming Sensitivity Experiments of Subtropical Cyclone Anita (2010) Under RCP 8.5 Scenario. *Journal of Geophysical Research: Atmospheres*, *126*(24). doi: 10.1029/2021JD035261

Noda, A. T., & Satoh, M. (2014). Intermodel variances of subtropical stratocumulus environments simulated in CMIP5 models. , 7754–7761. doi: 10.1002/2014GL061812.Received

Ohno, T., Noda, A. T., Seiki, T., & Satoh, M. (2021). Importance of Pressure Changes in High Cloud Area Feedback Due to Global Warming. *Geophysical Research Letters*, *48*(18). doi: 10.1029/2021GL093646

Ohno, T., & Satoh, M. (2018). Roles of Cloud Microphysics on Cloud Responses to Sea Surface Temperatures in Radiative-Convective Equilibrium Experiments Using a High-Resolution Global Nonhydrostatic Model. *Journal of Advances in Modeling Earth Systems*, *10*(8), 1970–1989. doi: 10.1029/2018MS001386

Ohno, T., Satoh, M., & Noda, A. (2019). Fine Vertical Resolution Radiative-Convective Equilibrium Experiments: Roles of Turbulent Mixing on the High-Cloud Response to Sea Surface Temperatures. *Journal of Advances in Modeling Earth Systems*, *11*(6), 1637–1654. doi: 10.1029/2019MS001704

Pichelli, E., Coppola, E., Sobolowski, S., Ban, N., Giorgi, F., Stocchi, P., . . . Vergara-Temprado, J. (2021, 6). The first multi-model ensemble of regional climate simulations at kilometer-scale resolution part 2: historical and future simulations of precipitation. *Climate Dynamics*, *56*(11-12), 3581–3602. Retrieved from `https://link.springer.com/10.1007/s00382-021-05657-4` doi: 10.1007/s00382-021-05657-4

Possner, A., Zubler, E., Fuhrer, O., Lohmann, U., & Schär, C. (2014, 4). A Case Study in Modeling Low-Lying Inversions and Stratocumulus Cloud Cover in the Bay of Biscay. *Weather and Forecasting*, *29*(2), 289–304. Retrieved from `https://journals.ametsoc.org/waf/article/29/2/289/39873/A-Case-Study-in-Modeling-LowLying-Inversions-and` doi: 10.1175/WAF-D-13-00039.1

Prein, A. F., Langhans, W., Fosser, G., Ferrone, A., Ban, N., Goergen, K., . . . Leung, R. (2015). A review on regional convection-permitting climate modeling: Demonstrations, prospects, and challenges. *Reviews of Geophysics*, *53*(2), 323–361. Retrieved from `http://dx.doi.org/10.1002/2014RG000475` doi: 10.1002/2014RG000475

Raschendorfer, M. (2001). The new turbulence parameterization of LM. *COSMO Newsletter*, *1*, 89–97.

Rasmussen, R., Liu, C., Ikeda, K., Gochis, D., Yates, D., Chen, F., . . . Gutmann, E. (2011, 6). High-Resolution Coupled Climate Runoff Simulations of Seasonal Snowfall over Colorado: A Process Study of Current and

Warmer Climate. *Journal of Climate*, *24*(12), 3015–3048. Retrieved from http://journals.ametsoc.org/doi/abs/10.1175/2010JCLI3985.1 doi: 10.1175/2010JCLI3985.1

Reinhardt, T., & Seifert, A. (2006). A three-category ice scheme for LMK. *COSMO Newsletter*, *6*, 115–120.

Ritter, B., & Geleyn, J.-F. (1992, 2). A Comprehensive Radiation Scheme for Numerical Weather Prediction Models with Potential Applications in Climate Simulations. *Monthly Weather Review*, *120*(2), 303–325. Retrieved from http://journals.ametsoc.org/doi/abs/10.1175/1520-0493(1992)120%3C0303:ACRSFN%3E2.0.CO;2%5Cnhttp://journals.ametsoc.org/doi/abs/10.1175/1520-0493%281992%29120%3C0303:ACRSFN%3E2.0.CO;2#.V5JN_92a2L0.mendeley%5Cnhttp://journals.ametsoc.org/doi/abs/10.1175/152 doi: 10.1175/1520-0493(1992)120⟨0303:ACRSFN⟩2.0.CO;2

Rockel, B., Will, A., & Hense, A. (2008, 8). The Regional Climate Model COSMO-CLM (CCLM). *Meteorologische Zeitschrift*, *17*(4), 347–348. Retrieved from http://www.schweizerbart.de/papers/metz/detail/17/56726/The_Regional_Climate_Model_COSMO_CLM_CCLM?af=crossref doi: 10.1127/0941-2948/2008/0309

Saint-Lu, M., Bony, S., & Dufresne, J. L. (2020). Observational Evidence for a Stability Iris Effect in the Tropics. *Geophysical Research Letters*, *47*(14). doi: 10.1029/2020GL089059

Sato, T., Kimura, F., & Kitoh, A. (2007, 1). Projection of global warming onto regional precipitation over Mongolia using a regional climate model. *Journal of Hydrology*, *333*(1), 144–154. doi: 10.1016/j.jhydrol.2006.07.023

Satoh, M., Iga, S. I., Tomita, H., Tsushima, Y., & Noda, A. T. (2012). Response of upper clouds in global warming experiments obtained using a global nonhydrostatic model with explicit cloud processes. *Journal of Climate*, *25*(6), 2178–2191. doi: 10.1175/JCLI-D-11-00152.1

Satoh, M., Stevens, B., Judt, F., Khairoutdinov, M., Lin, S.-j., Putman, W. M., & Düben, P. (2019, 9). Global Cloud-Resolving Models. *Current Climate Change Reports*, *5*(3), 172–184. Retrieved from http://link.springer.com/10.1007/s40641-019-00131-0 doi: 10.1007/s40641-019-00131-0

Schär, C., Frei, C., Lüthi, D., & Davies, H. C. (1996, 3). Surrogate climate-change scenarios for regional climate models. *Geophysical Research Letters*, *23*(6), 669–672. Retrieved from `http://doi.wiley.com/10.1029/96GL00265` doi: 10.1029/96GL00265

Schär, C., Fuhrer, O., Arteaga, A., Ban, N., Charpilloz, C., Di Girolamo, S., ... Wernli, H. (2020, 5). Kilometer-scale climate models: Prospects and challenges. *Bulletin of the American Meteorological Society*, *101*(5), E567-E587. Retrieved from `https://journals.ametsoc.org/bams/article/101/5/E567/345557/KilometerScale-Climate-Models-Prospects-and` doi: 10.1175/BAMS-D-18-0167.1

Schlemmer, L., Schär, C., Lüthi, D., & Strebel, L. (2018, 8). A Groundwater and Runoff Formulation for Weather and Climate Models. *Journal of Advances in Modeling Earth Systems*, *10*(8), 1809–1832. Retrieved from `http://doi.wiley.com/10.1029/2017MS001260` doi: 10.1029/2017MS001260

Schneider, T., Teixeira, J., Bretherton, C. S., Brient, F., Pressel, K. G., Schär, C., & Siebesma, A. P. (2017). Climate goals and computing the future of clouds. *Nature Climate Change*, *7*(1). doi: 10.1038/nclimate3190

Schulz, H., Eastman, R., & Stevens, B. (2021, 9). Characterization and Evolution of Organized Shallow Convection in the Downstream North Atlantic Trades. *Journal of Geophysical Research: Atmospheres*, *126*(17). doi: 10.1029/2021JD034575

Sherwood, S. C., Bony, S., & Dufresne, J.-L. (2014, 1). Spread in model climate sensitivity traced to atmospheric convective mixing. *Nature*, *505*(7481), 37–42. Retrieved from `http://www.nature.com/articles/nature12829` doi: 10.1038/nature12829

Shine, K. P., Bourqui, M. S., de Forster, P. M., Hare, S. H., Langematz, U., Braesicke, P., ... Schwarzkopf, M. D. (2003, 4). A comparison of model-simulated trends in stratospheric temperatures. *Quarterly Journal of the Royal Meteorological Society*, *129*(590 PART A), 1565–1588. doi: 10.1256/qj.02.186

Singh, M. S., & O'Gorman, P. A. (2015, 10). Increases in moist-convective updraught velocities with warming in radiative-convective equilibrium. *Quarterly Journal of the Royal Meteorological Society*, *141*(692), 2828–2838. doi: 10.1002/qj.2567

Song, X., & Zhang, G. J. (2018, 3). The Roles of Convection Parameterization in the Formation of Double ITCZ Syndrome in the NCAR CESM: I. Atmospheric Processes. *Journal of Advances in Modeling Earth Systems*, *10*(3), 842–866. Retrieved from https://onlinelibrary.wiley.com/doi/10.1002/2017MS001191 doi: 10.1002/2017MS001191

Sørland, S. L., Brogli, R., Pothapakula, P. K., Russo, E., Van de Walle, J., Ahrens, B., ... Thiery, W. (2021, 8). COSMO-CLM regional climate simulations in the Coordinated Regional Climate Downscaling Experiment (CORDEX) framework: a review. *Geoscientific Model Development*, *14*(8), 5125–5154. Retrieved from https://gmd.copernicus.org/articles/14/5125/2021/ doi: 10.5194/gmd-14-5125-2021

Stevens, B. (2007, 8). On the Growth of Layers of Nonprecipitating Cumulus Convection. *Journal of the Atmospheric Sciences*, *64*(8), 2916–2931. Retrieved from http://journals.ametsoc.org/doi/abs/10.1175/JAS3983.1https://journals.ametsoc.org/doi/10.1175/JAS3983.1 doi: 10.1175/JAS3983.1

Stevens, B., Acquistapace, C., Hansen, A., Heinze, R., Klinger, C., Klocke, D., ... ZÄNGL, G. (2020). The Added Value of Large-eddy and Storm-resolving Models for Simulating Clouds and Precipitation. *Journal of the Meteorological Society of Japan. Ser. II*, *98*(2), 395–435. Retrieved from https://www.jstage.jst.go.jp/article/jmsj/98/2/98_2020-021/_article doi: 10.2151/jmsj.2020-021

Stevens, B., Moeng, C.-H., Ackerman, A. S., Bretherton, C. S., Chlond, A., de Roode, S., ... Zhu, P. (2005, 6). Evaluation of Large-Eddy Simulations via Observations of Nocturnal Marine Stratocumulus. *Monthly Weather Review*, *133*(6), 1443–1462. Retrieved from http://journals.ametsoc.org/doi/10.1175/MWR2930.1 doi: 10.1175/MWR2930.1

Stevens, B., Satoh, M., Auger, L., Biercamp, J., Bretherton, C. S., Chen, X., ... Zhou, L. (2019, 12). DYAMOND: the DYnamics of the Atmospheric general circulation Modeled On Non-hydrostatic Domains. *Progress in Earth and Planetary Science*, *6*(1), 61. Retrieved from https://progearthplanetsci.springeropen.com/articles/10.1186/s40645-019-0304-z doi: 10.1186/s40645-019-0304-z

Suhas, E., & Zhang, G. J. (2015). Evaluating convective parameterization closures using cloud-resolving model simulation of tropical deep convection. *Journal of*

Geophysical Research, *120*(4), 1260–1277. doi: 10.1002/2014JD022246

Taylor, K. E., Stouffer, R. J., & Meehl, G. A. (2012, 4). An Overview of CMIP5 and the Experiment Design. *Bulletin of the American Meteorological Society*, *93*(4), 485–498. Retrieved from `https://journals.ametsoc.org/doi/10.1175/BAMS-D-11-00094.1` doi: 10.1175/BAMS-D-11-00094.1

Tegen, I., Hollrig, P., Chin, M., Fung, I., Jacob, D., & Penner, J. (1997, 10). Contribution of different aerosol species to the global aerosol extinction optical thickness: Estimates from model results. *Journal of Geophysical Research Atmospheres*, *102*(20), 23895–23915. doi: 10.1029/97jd01864

Tian, B. (2015, 5). Spread of model climate sensitivity linked to double-Intertropical Convergence Zone bias. *Geophysical Research Letters*, *42*(10), 4133–4141. doi: 10.1002/2015GL064119

Tsushima, Y., Iga, S.-i., Tomita, H., Satoh, M., Noda, A. T., & Webb, M. J. (2014, 9). High cloud increase in a perturbed SST experiment with a global non-hydrostatic model including explicit convective processes. *Journal of Advances in Modeling Earth Systems*, *6*(3), 571–585. Retrieved from `http://doi.wiley.com/10.1002/2013MS000301` doi: 10.1002/2013MS000301

Vergara-Temprado, J., Ban, N., Panosetti, D., Schlemmer, L., & Schär, C. (2020, 3). Climate Models Permit Convection at Much Coarser Resolutions Than Previously Considered. *Journal of Climate*, *33*(5), 1915–1933. Retrieved from `http://journals.ametsoc.org/doi/10.1175/JCLI-D-19-0286.1` doi: 10.1175/JCLI-D-19-0286.1

Vial, J., Bony, S., Dufresne, J., & Roehrig, R. (2016, 12). Coupling between lower-tropospheric convective mixing and low-level clouds: Physical mechanisms and dependence on convection scheme. *Journal of Advances in Modeling Earth Systems*, *8*(4), 1892–1911. Retrieved from `https://onlinelibrary.wiley.com/doi/abs/10.1002/2016MS000740` doi: 10.1002/2016MS000740

Vial, J., Bony, S., Stevens, B., & Vogel, R. (2017). Mechanisms and Model Diversity of Trade-Wind Shallow Cumulus Cloud Feedbacks: A Review. *Surveys in Geophysics*, *38*(6), 1331–1353. doi: 10.1007/s10712-017-9418-2

von Storch, J.-S., Putrasahan, D., Lohmann, K., Gutjahr, O., Jungclaus, J., Bittner, M., … Roeckner, E. (2017). *MPI-M MPIESM1.2-HR model output prepared for CMIP6 HighResMIP.* Earth System Grid Federation. Retrieved from https://doi.org/10.22033/ESGF/CMIP6.762 doi: 10.22033/ESGF/CMIP6.762

Waliser, D. E., & Gautier, C. (1993, 11). A Satellite-derived Climatology of the ITCZ. *Journal of Climate*, *6*(11), 2162–2174. Retrieved from http://journals.ametsoc.org/doi/10.1175/1520-0442(1993)006<2162:ASDCOT>2.0.CO;2 doi: 10.1175/1520-0442(1993)006⟨2162:ASDCOT⟩2.0.CO;2

Warren, S., Hahn, C., London, J., Chervin, R., & Jenne, R. (1988, 12). *Global distribution of total cloud cover and cloud type amounts over the ocean* (Tech. Rep.). USDOE Office of Energy Research (ER). Retrieved from http://www.osti.gov/servlets/purl/5415329-XbAE7q/ doi: 10.2172/5415329

Webb, M. J., Andrews, T., Bodas-Salcedo, A., Bony, S., Bretherton, C. S., Chadwick, R., ... Watanabe, M. (2017). The Cloud Feedback Model Intercomparison Project (CFMIP) contribution to CMIP6. *Geoscientific Model Development*, *10*(1). doi: 10.5194/gmd-10-359-2017

Webb, M. J., & Lock, A. P. (2020, 9). Testing a Physical Hypothesis for the Relationship Between Climate Sensitivity and Double-ITCZ Bias in Climate Models. *Journal of Advances in Modeling Earth Systems*, *12*(9), 4133–4141. Retrieved from https://onlinelibrary.wiley.com/doi/10.1029/2019MS001999 doi: 10.1029/2019MS001999

Wicker, L. J., & Skamarock, W. C. (2002, 8). Time-Splitting Methods for Elastic Models Using Forward Time Schemes. *Monthly Weather Review*, *130*(8), 2088–2097. Retrieved from https://doi.org/10.1175/1520-0493(2002)130%3C2088:TSMFEM%3E2.0.COhttp://0.0.0.2 doi: 10.1175/1520-0493(2002)130⟨2088:TSMFEM⟩2.0.CO;2

Wing, A. A., Stauffer, C. L., Becker, T., Reed, K. A., Ahn, M. S., Arnold, N. P., ... Zhao, M. (2020). Clouds and Convective Self-Aggregation in a Multimodel Ensemble of Radiative-Convective Equilibrium Simulations. *Journal of Advances in Modeling Earth Systems*, *12*(9), 1–38. doi: 10.1029/2020MS002138

Wodzicki, K. R., & Rapp, A. D. (2016). Long-term characterization of the Pacific ITCZ using TRMM, GPCP, and ERA-Interim. *Journal of Geophysical Research*, *121*(7), 3153–3170. doi: 10.1002/2015JD024458

Wood, R. (2012, 8). Stratocumulus Clouds. *Monthly Weather Review*, *140*(8), 2373–2423. Retrieved from http://journals.ametsoc.org/doi/abs/10.1175/

MWR-D-11-00121.1https://journals.ametsoc.org/mwr/article/140/8/2373/71595/Stratocumulus-Clouds doi: 10.1175/MWR-D-11-00121.1

Wu, W., & Lynch, A. H. (2000, 9). Response of the seasonal carbon cycle in high latitudes to climate anomalies. *Journal of Geophysical Research: Atmospheres*, *105*(D18), 22897–22908. doi: 10.1029/2000JD900340

Zelinka, M. D., Randall, D. A., Webb, M. J., & Klein, S. A. (2017, 10). Clearing clouds of uncertainty. *Nature Climate Change*, *7*(10), 674–678. Retrieved from http://www.nature.com/articles/nclimate3402 doi: 10.1038/nclimate3402

Zelinka, M. D., Zhou, C., & Klein, S. A. (2016, 9). Insights from a refined decomposition of cloud feedbacks. *Geophysical Research Letters*, *43*(17), 9259–9269. Retrieved from http://doi.wiley.com/10.1002/2016GL069917 doi: 10.1002/2016GL069917

Zeman, C., Wedi, N. P., Dueben, P. D., Ban, N., & Schär, C. (2021, 7). Model intercomparison of COSMO 5.0 and IFS 45r1 at kilometer-scale grid spacing. *Geoscientific Model Development*, *14*(7), 4617–4639. doi: 10.5194/gmd-14-4617-2021

Zhang, G. J., Song, X., & Wang, Y. (2019, 11). The double ITCZ syndrome in GCMs: A coupled feedback problem among convection, clouds, atmospheric and ocean circulations. *Atmospheric Research*, *229*(December 2018), 255–268. Retrieved from https://doi.org/10.1016/j.atmosres.2019.06.023https://linkinghub.elsevier.com/retrieve/pii/S0169809518316788 doi: 10.1016/j.atmosres.2019.06.023

Zhou, W., Leung, L. R., Lu, J., Yang, D., & Song, F. (2020, 11). Contrasting Recent and Future ITCZ Changes From Distinct Tropical Warming Patterns. *Geophysical Research Letters*, *47*(22). doi: 10.1029/2020GL089846

Zuidema, P., Redemann, J., Haywood, J., Wood, R., Piketh, S., Hipondoka, M., & Formenti, P. (2016, 7). Smoke and Clouds above the Southeast Atlantic: Upcoming Field Campaigns Probe Absorbing Aerosol's Impact on Climate. *Bulletin of the American Meteorological Society*, *97*(7), 1131–1135. Retrieved from https://journals.ametsoc.org/doi/10.1175/BAMS-D-15-00082.1 doi: 10.1175/BAMS-D-15-00082.1

Supporting Information for "Application of the Pseudo-Global Warming Approach in a Kilometer-Resolution Climate Simulation of the Tropics"

Christoph Heim[1], David Leutwyler[1], Christoph Schär[1]

[1]Institute for Atmospheric and Climate Science, ETH Zurich, Zürich, Switzerland

Contents of this file

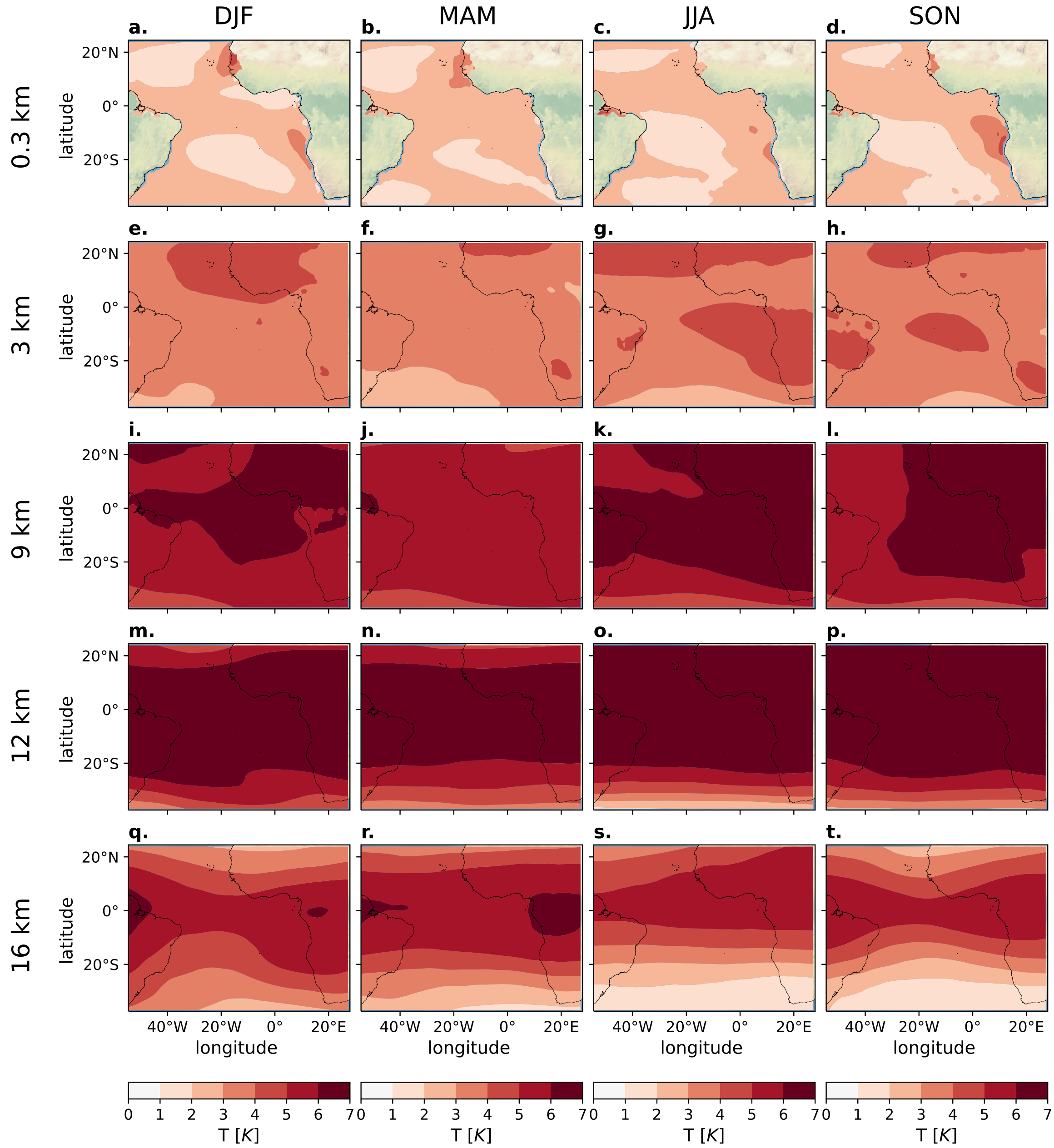

Figure S1. Climate delta for temperature shown at (first row) 0.3 km, (second row) 3 km, (third row) 9 km, (fourth row) 12 km, and (fifth row) 16 km altitude for the seasons (first column) December-February, (second column) March-May, (third column) June-August, and (fourth column) September-November. The delta is computed as the difference between SCEN (SSP5-8.5, 2070-2099) and HIST (historical, 1985-2014) for the MPI-ESM1-2-HR model.

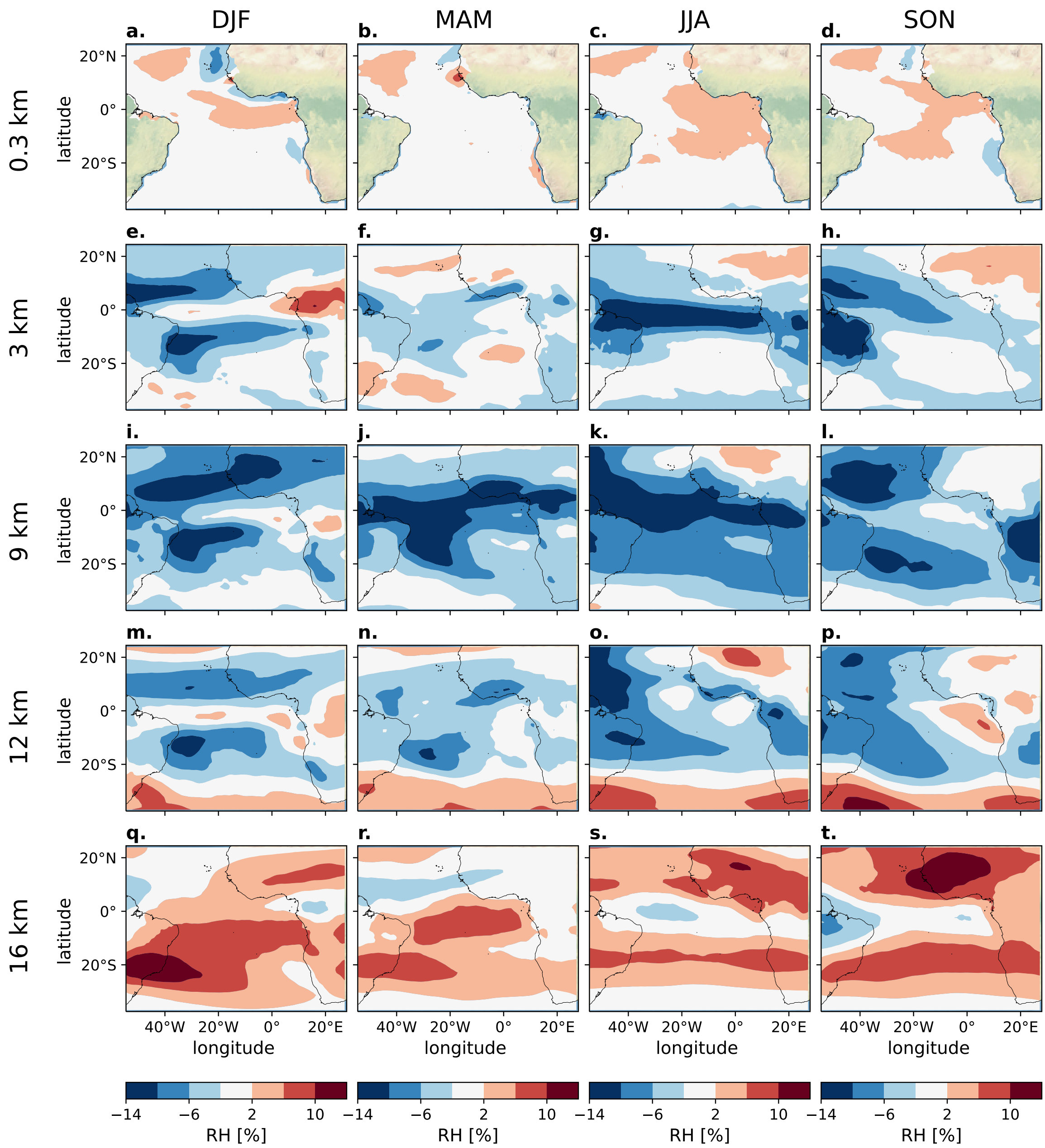

Figure S2. As Fig. S1 but shown for the relative humidity.

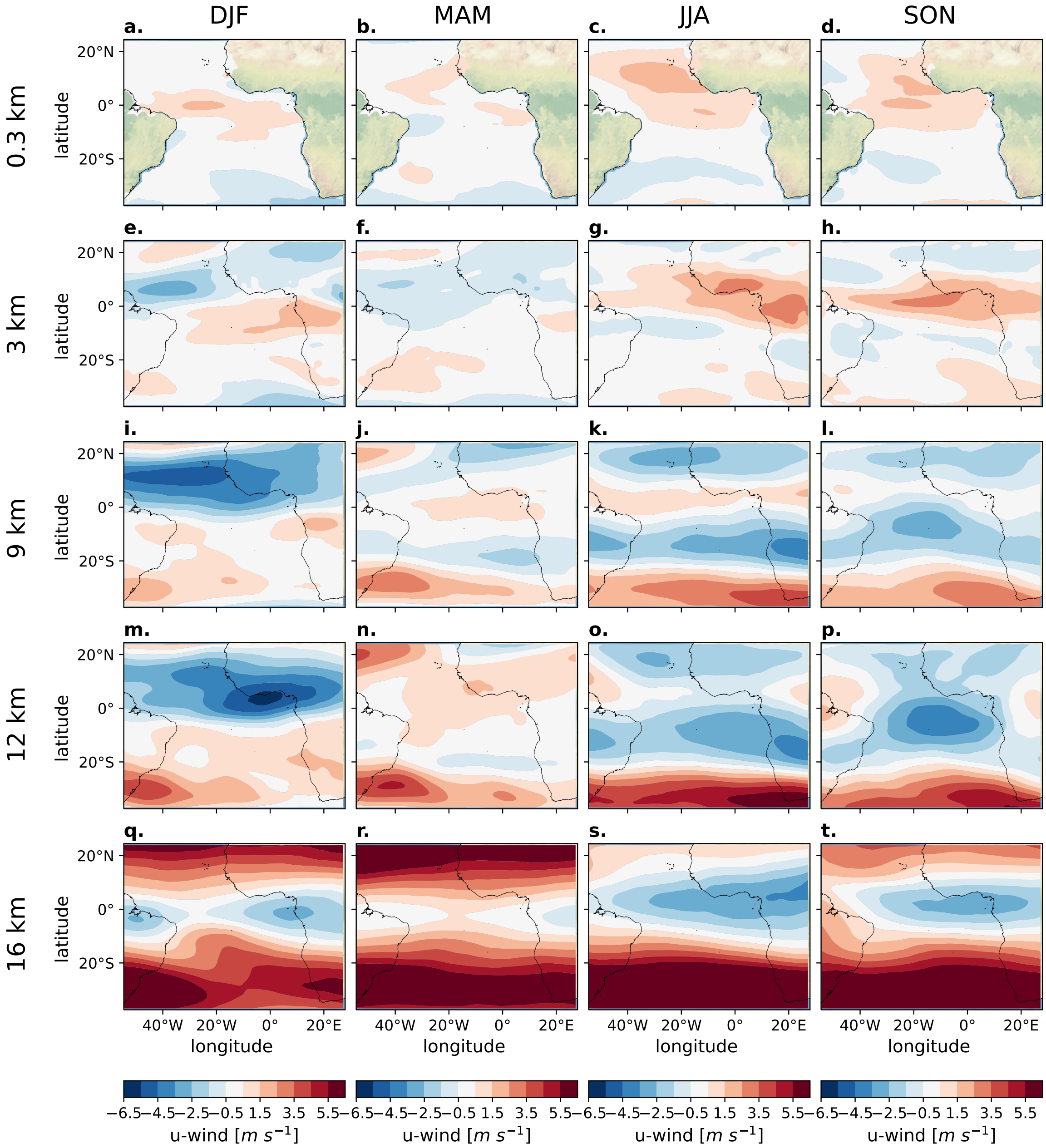

Figure S3. As Fig. S1 but shown for the zonal wind.

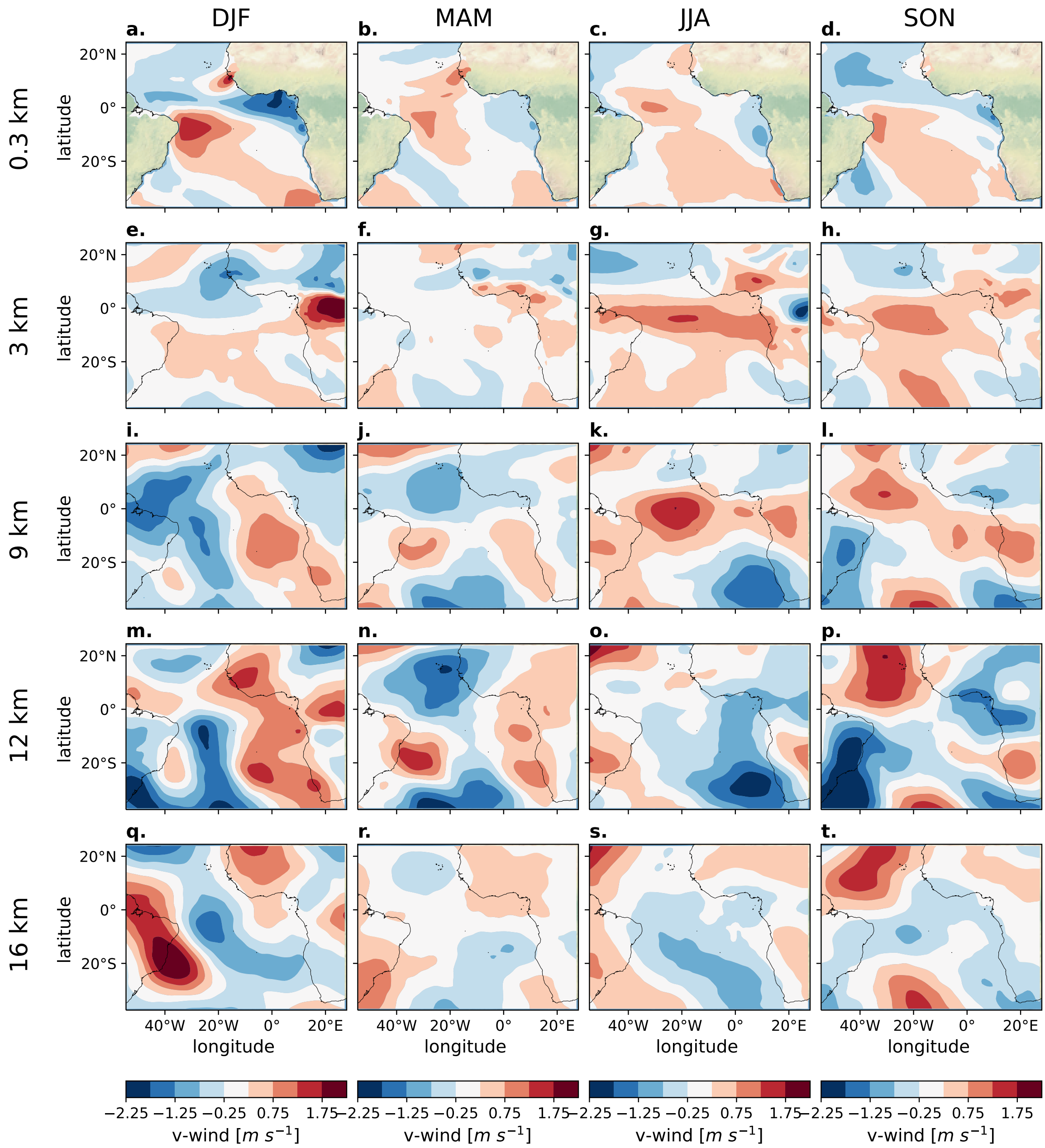

Figure S4. As Fig. S1 but shown for the meridional wind.

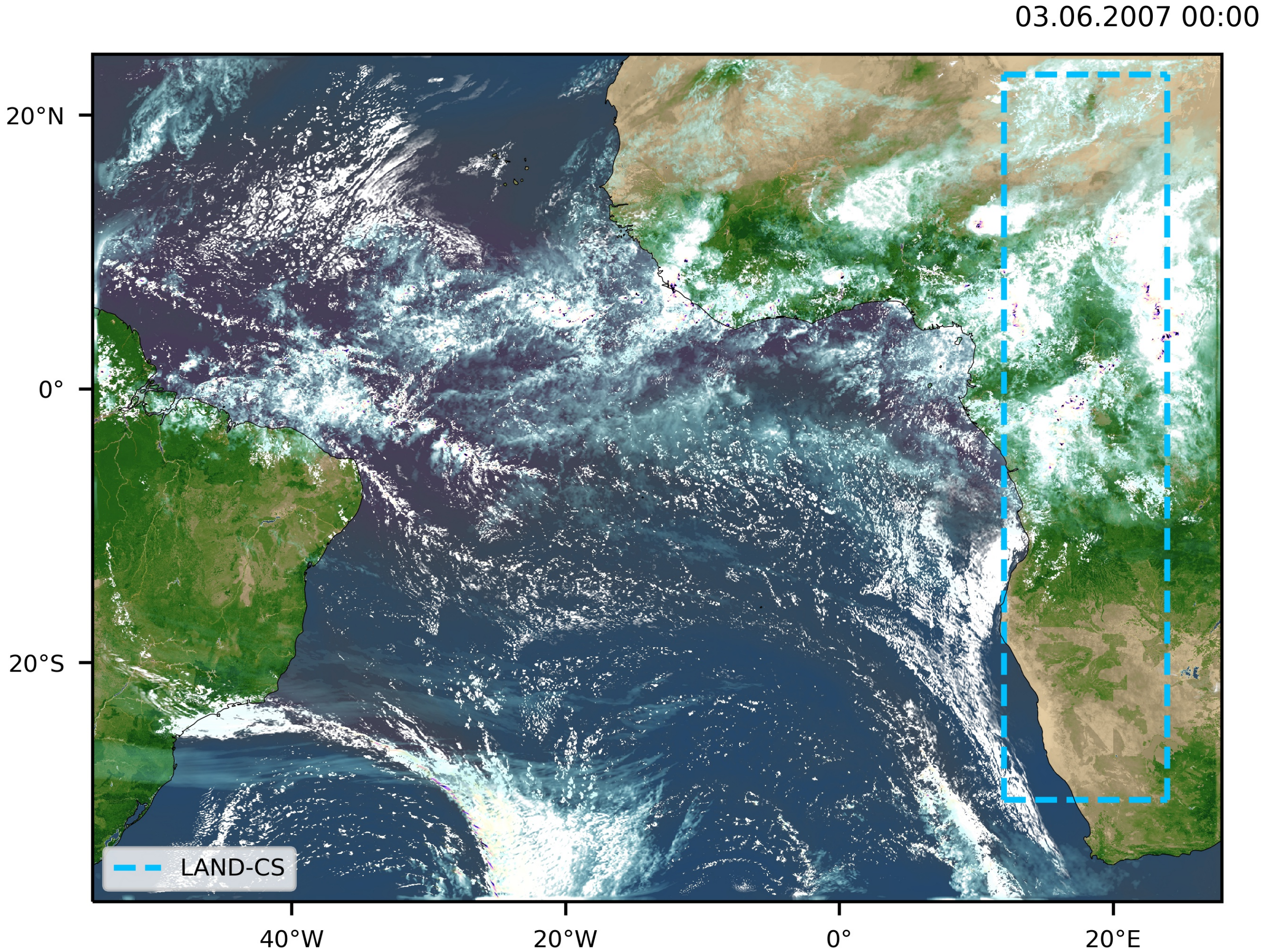

Figure S5. Simulation visualization and LAND-CS analysis domain used in supplementary Fig. S6.

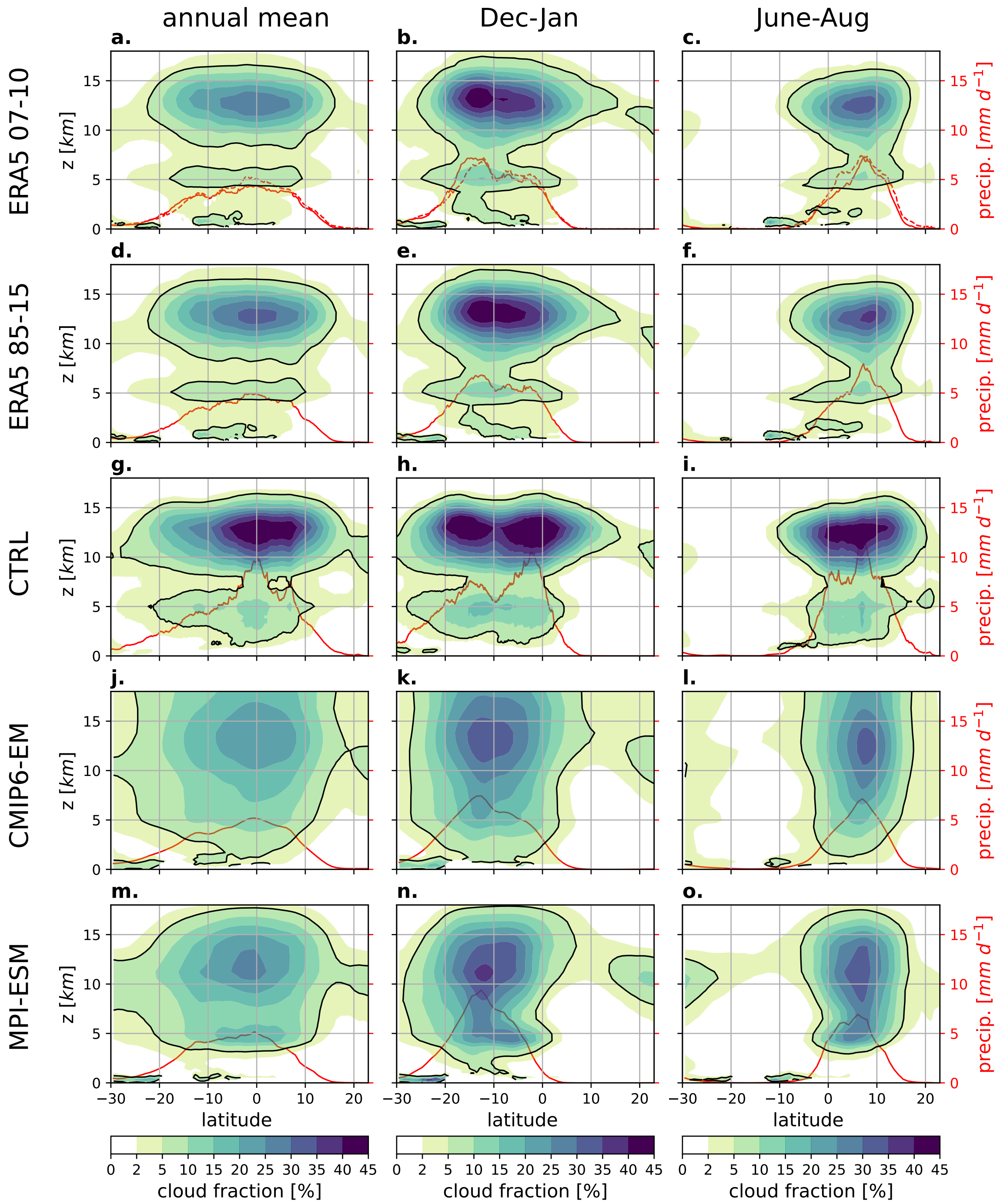

Figure S6. Altitude-latitude cross-sections of the cloud fraction [%] (green-to-blue contours) averaged along the longitudes of the LAND-CS domain. The black contour lines locate the 5% cloud fraction level. The solid red lines show surface precipitation [mm d^{-1}] represented on the right y-axis. The panels show (a-c) ERA5 (2007-2010), (d-f) ERA5 (1985-2014), (g-i) CTRL (2007-2010), (j-l) CMIP6-EM HIST (1985-2014), and (m-o) MPI-ESM HIST (1985-2014). The values represent multi-year averages (left panels) during the entire year, as well as (middle panels) during December, January, February and (right panels) June, July, August when the continental ITCZ reaches its southernmost and northernmost extent, respectively. As a complementary reference observation, GPM IMERG precipitation is shown as a red dashed line in panels (a-c).

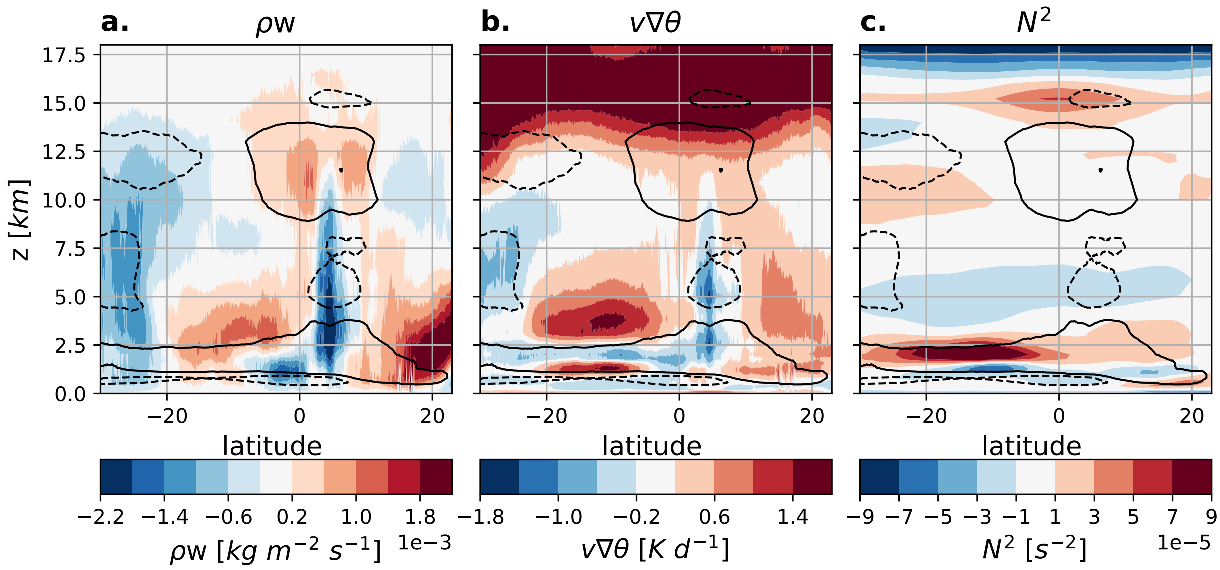

Figure S7. Altitude-latitude cross-sections of the difference CTRL−ERA5 (2007-2010) in (a) the vertical mass flux [kg m^{-2} s^{-1}], (b) the diabatic heating rate $\dot{\theta}$ [K d^{-1}] approximated by $\dot{\theta} \approx \mathbf{v} \cdot \nabla\theta$., and (c) the Brunt-Väisälä frequency [s^{-1}] along the longitudes of the HC-CS domain. The black contour lines indicate the 2% level of difference in the cloud fraction level where solid (dashed) lines represent a positive (negative) difference. The comparison of all panels reveals that the weaker subsidence in the lower subtropical free troposphere in CTRL compared to ERA5 results from a weaker diabatic cooling rather than increased stability. The stability of the lower free troposphere is lower in CTRL than in ERA5.